Instituto Universitário de Lisboa

Department of Information Science and Technology

Transmission of PAM4 signals in intra-datacenters connections with direct-detection and multicore fibers limited by inter-core crosstalk

Inês Costa Jorge

A Dissertation presented in partial fulfillment of the Requirements for the Degree of

Master in Telecommunications and Computer Engineering

Supervisor

Prof. Dr. João Rebola, Assistant Professor

ISCTE - Instituto Universitário de Lisboa

Co-Supervisor

Prof. Dr. Adolfo Cartaxo, Full Professor

ISCTE - Instituto Universitário de Lisboa

September 2019

Resumo

Actualmente, o tráfego nos centros de dados tem aumentado dramaticamente nos últimos anos. Como tal, é necessário uma grande evolução nas ligações dos centros de dados para acomodar esse aumento de tráfego. A solução proposta neste trabalho é usar a modulação de amplitude por impulsos com quatro níveis (PAM4) e fibras multinúcleo (MCFs) para suportar ligações dentro de centro de dados. Contudo, a transmissão nas MCFs é significativamente degradada pela diafonia entre núcleos (ICXT). Neste trabalho, o impacto da ICXT no desempenho de sistemas PAM4 correspondentes a ligações curtas com detecção direta, emulando ligações dentro de centros de dados é analisado. Para avaliar o impacto da ICXT no desempenho do sistema, várias métricas são usadas como: análise do diagrama de olho, taxa de erro bit, penalidade de potência e probabilidade de indisponibilidade (OP).

Os resultados numéricos mostram que os níveis de ICXT que conduzem à degradação da penalidade de potência de 1 dB com um produto ritmo de símbolo-*skew* baixo estão, pelo menos, 2.3 dB acima dos valores encontrados com um produto ritmo de símbolo-*skew* elevado. Para estes níveis de ICXT, o sistema PAM4 apresenta-se indisponível com uma OP acima de 10^{-2}. Assim demonstra-se que a OP é uma métrica de desempenho essencial relativamente à penalidade de potência de 1 dB para garantir a qualidade de serviço em sistemas PAM4 com deteção direta e suportados por fibras multinúcleo. Além disso, comparando com os sistemas OOK, é necessário um nível ICXT acima de 7.6 dB para obter a mesma OP no sistema PAM4.

Palavras-chave: diafonia entre núcleos, fibra multinúcleo, indisponibilidade, ligações em centros de dados, PAM4, penalidade de potência, taxa de erro de bit.

Abstract

Nowadays, traffic in datacenters has been dramatically increasing over the last few years. As such, it is necessary to scale the connections of the datacenters, to accommodate such increase of traffic. The solution proposed in this work is to use four-level pulse amplitude modulation (PAM4) and multicore fibers (MCFs) to support intra-datacenters connections. However, transmission in MCFs is significantly degraded by inter-core crosstalk (ICXT) between cores. In this work, the impact of ICXT on the performance of PAM4 transmission in short-haul direct-detection links, emulating intra-datacenters connections, is analyzed. To evaluate the ICXT impact on the performance of the system, several metrics are used such as: bit error rate, eye-pattern analysis, power penalty and outage probability (OP).

Our numerical results show that the ICXT levels that lead to 1 dB power penalty degradation with low skew-symbol rate product are at least 2.3 dB above the ones found with high skew-symbol rate product. For these crosstalk levels, the PAM4 system is probably unavailable with an OP above 10^{-2}. To reach an acceptable reference OP of 3.8×10^{-3}, the ICXT level must be reduced at least 5 dB, when compared to the ICXT level that leads to the 1 dB power penalty. Hence, the OP is an essential performance metric instead of the 1 dB power penalty to guarantee quality of service in PAM4 direct-detection systems supported by MCFs. Furthermore, comparing to OOK systems, a much higher ICXT level above 7.6 dB is required to achieve the same OP in the PAM4 system.

Keywords: bit error rate, inter-core crosstalk, intra-datacenters connections, multicore fiber, outage probability, PAM4, power penalty.

Acknowledgements

For all their support, knowledge and advises, firstly I would like to acknowledge to my supervisors Professor João Rebola and Professor Adolfo Cartaxo, that helped me in the development and completion of this dissertation. Also, I want to thank Instituto de Telecomunicações (IT)-IUL, for providing access to their installations and the material.

I want to thank my family for always supporting me in my decisions, for all the motivation they gave me during these years and for always trusting me.

Finally, I want to thank my boyfriend for all the patience, motivation, support and help during all this time.

Contents

List of Figures

List of Tables

List of Acronyms

ASE	**A**mplified **S**pontaneous **E**mission
AWGN	**A**dditive **W**hite **G**aussian **N**oise
BER	**B**it **E**rror **R**ate
B2B	**B**ack-**t**o-**B**ack
CAGR	**C**ompound **A**nual **G**rowth **R**ate
CD	**C**hromatic **D**ispersion
DCM	**D**iscrete **C**hanges **M**odel
DSF	**D**ispersion-**S**hifted **F**iber
DSP	**D**igital **S**ignal **P**rocessing
EB	**E**xa**B**yte
EDFA	**E**rbium-**D**oped **F**iber **A**mplifier
FEC	**F**orward **E**rror **C**orrection
FMF	**F**ew-**M**ode **F**iber
FWM	**F**our-**W**ave **M**ixing
ICXT	**I**ntercore **C**rosstalk
IoT	**I**nternet of **T**hings
ISI	**I**ntersymbol **I**nterference
MCF	**M**ulticore **F**iber
MMF	**M**ultimode **F**iber
MIMO	**M**ultiple **I**n **M**ultiple **O**ut
NEP	**N**oise **E**quivalent **P**ower
NRZ	**N**on **R**eturn-to-**Z**ero
OCT	**O**uter **C**ladding **T**hickness

OOK	**O**n-**O**ff **K**eying
OP	**O**utage **P**robability
PAM4	**P**ulse **A**mplitude **M**odulation with **4** levels
PDI	**P**ropagation-**D**irection **I**nterleaving
PMD	**P**olarization **M**ode **D**ispersion
PMP	**P**hase **M**atching **P**oint
RPS	**R**andom **P**hase **S**hift
SBS	**S**timulated **B**rillouin **S**cattering
SCF	**S**ingle **C**ore **F**iber
SC-SMF	**S**ingle **C**ore-**S**inglemode **F**iber
SDM	**S**pace **D**ivision **M**ultiplexing
SMF	**S**ingle **M**ode **F**iber
SPM	**S**elf-**P**hase **M**odulation
SRS	**S**timulated **R**aman **S**cattering
ToR	**T**op **o**f **R**ack
WAN	**W**ide **A**rea **N**etwork
WDM	**W**avelength **D**ivision **M**ultiplexing
XPM	**C**ross **P**hase **M**odulation

List of Symbols

a_k	Transmitted PAM4 symbol
A	Normalized amplitude level corresponding to symbol '1'
$B_{e,n}$	Noise equivalent bandwidth of the electrical filter
B_n	n-th order Bessel polynomial
$\overline{\beta}_m$	Average of the propagation constants of both polarizations in core m
$\overline{\beta}_n$	Average of the propagation constants of both polarizations in core n
C	Normalized amplitude level corresponding to symbol '2'
$c_F(t)$	PAM4 signal at the output of the interfered core n
$c_{F,x}(t)$	PAM4 signal at the output of the interfered core n in polarization $\mathbf{x}$
$c_{F,y}(t)$	PAM4 signal at the output of the interfered core n in polarization $\mathbf{y}$
$c_m(t)$	PAM4 signal at the input of the interfering core m
$c_{m,x}(t)$	PAM4 signal at the input of the core interfering m in polarization $\mathbf{x}$
$c_{m,y}(t)$	PAM4 signal at the input of the interfering core m in polarization $\mathbf{y}$
$c_n(t)$	PAM4 signal at the input of the interfered core n
$c_{n,x}(t)$	PAM4 signal at the input of the interfered core n in polarization $\mathbf{x}$
$c_{n,y}(t)$	PAM4 signal at the input of the interfered core n in polarization $\mathbf{y}$
$c_{PIN}(t)$	Signal at the output of the PIN photodetector
$c_{XT}(t)$	ICXT signal at the output of the interfering core m
$c_{XT,x}(t)$	ICXT signal at the output of the interfering core m in polarization x
$c_{XT,y}(t)$	ICXT signal at the output of the interfering core m in polarization y
D_λ	Dispersion parameter
e_i	Normalized eye opening
$\mathcal{F}^{-1}\{\ \}$	Inverse Fourier transform

f	Lowpass equivalent frequency
f_{-3dB}	-3 dB cutoff frequency
$F_{a,b}(\omega)$	ICXT transfer function in polarization directions **a** and **b**
$F_{x,x}(\omega)$	ICXT transfer function from polarization direction **x** to **x**
$F_{x,y}(\omega)$	ICXT transfer function from polarization direction **x** to **y**
$F_{y,x}(\omega)$	ICXT transfer function from polarization direction **y** to **x**
$F_{y,y}(\omega)$	ICXT transfer function from polarization direction **y** to **y**
F_i	Optimized decision threshold with i=1,2,3
$F_{n,i}$	Normalized decision threshold with i=1,2,3
h	Planck constant
$H_F(\omega)$	Linear propagation transfer function of the fiber
$i_{i,k}$	Current at the input of the decision circuit with i=0,1,2,3
$\overline{K}_{nm}$	Average inter-core coupling coefficient of both polarization directions
L	Fiber length
M	Time misalignment ratio
n	Order of the Bessel filter
N	Number of generated PAM4 symbols in each MCF realization
N_b	Number of the bits of the offset register
N_c	Number of interfering cores
N_o	Number of occurrences of BER above the BER limit
N_p	Number of PMPs
N_r	Number of simulated realizations
N_s	Number of samples per symbol
$\overline{P_{av}}$	Average power of the PAM4 optical signal in the optical transmitter
P_i	Theoretical power corresponding to the transmitted i-th symbol
q	Charge of the electron
$Q_n(s)$	n-th order polynomial factor
r	Extinction ratio
R_s	Symbol rate
R_λ	PIN responsivity
S_{mn}	MCF skew parameter

T_s	Symbol period
X_c	Crosstalk level at the MCF output
z_k	Longitudinal coordinate corresponding to the k-th PMP
t	Time
ξ_m	Variable between 0 and 1 that controls the power distribution between polarizations in core m
ξ_n	Variable between 0 and 1 that controls the power distribution between polarizations in core n
η	Photodetector efficiency
λ	Carrier wavelength
ν	Optical frequency of the incident optical power
σ_c^2	Power of the thermal noise
$\sigma_{i,k}$	Noise standard deviation of the current at the input of the decision circuit with i=0,1,2,3
$\phi_{nm,k}$	RPS associated with the k-th PMP
ω	Angular frequency

Chapter 1

Introduction

This dissertation focuses on the performance evaluation of short-haul direct-detection optical links typically used in intra-datacenters connections supported by multicore fibers (MCFs) with four-level pulse amplitude modulation (PAM4) signals transmission, where inter-core crosstalk (ICXT) is the dominant performance limitation. Particularly, the ICXT maximum level acceptable to not exceed a given outage probability (OP) and the performance comparison with on-off keying (OOK) signals transmission are assessed throughout this work.

1.1 Motivation

Datacenters provide an infrastructure to Internet online services such as web-browsing, e-mail, video-streaming, storage and file sharing, cloud computing and mobile services. Due to all these services and the emergence of 5G and Internet of Things (IoT), traffic in datacenters has been dramatically increasing over the last few years [1]. With the growth of demanding capacity in datacenters, data traffic, which was mainly transmitted only from external datacenters to servers, started to be transfered between servers inside the same datacenter or anothers nearby supported by the optical fibers technology. One of the current solutions to scale the capacity of datacenters connections is the use of multiple wavelengths to carry

Wavelength Division Multiplexing (WDM) channels, each channel composed by an OOK signal. WDM is the technology that allows signals with different wavelengths to be sent through a single optical fiber. OOK is the simplest modulation format, however it leads to the lowest channel capacity. In 2007, the first generation of intra-datacenters technology operated at 10 Gb/s using 1 WDM channel, OOK modulation, direct-detection and a single wavelength was released [2]. In 2010, the technology has evolved into a second generation and operated at a 40 Gb/s aggregate bit rate with 4 WDM channels [2]. The third generation, from 2014, operated at 100 Gb/s with 4 WDM channels each one at 25 Gb/s with OOK transmission [2]. In 2017, a generation of 400 Gb/s datacenters connections emerged, employing the more bandwidth-efficient PAM4, doubled the WDM channels in use to 8 and the data rate in each channel from 25 Gb/s to 50 Gb/s, leading to an aggregate rate of 400 Gb/s [2]. The PAM4 format is seen as cost-effective and efficient enabler of 100G and 400G per channel in datacenters connections [3]. So, in the future, it is expected that PAM4 supported systems can lead to data rates of 800 Gb/s and 1.6 Tb/s in the datacenters connections [2].

The connections between datacenters can be classified into intra-datacenters connections, which have a range up to 10 km or inter-datacenters connections that have a range up to 100 km [3]. The transmission in the datacenters is mainly done through the use of single-core single-mode fibers (SC-SMF). Recent SC-SMF transmissions have achieved a transmission capacity about 100 Tb/s and a capacity-distance product over 100 Pb/s·km relying on the use of optical coherent-detection allied with digital signal processing (DSP) [4]. However, datacenters connections are still exploring optical direct-detection systems due to its lower cost and simplicity. For the sake of saving space between the racks inside datacenters, reducing fiber per area density, and to reduce inventory issues, MCFs are one of the most attractive technologies to overcome the use of SC-SMF in intra-datacenters connections [5]. In this work, homogeneous weakly-coupled MCFs are proposed and studied for the intra-datacenters connections, since in these fibers, each core has similar properties, as geometry and refractive index, all the cores have the

same propagation constant and can be used as independent transmission channels [6], [7].

However, transmission in homogeneous MCFs is impaired by ICXT. There is a degradation of system performance caused by ICXT, which can significantly limit the short-haul direct-detection system performance and the transmission distance in datacenters connections or lead to long time periods of service outage [8]. So, it is essential to study the OP in PAM4 direct-detection systems supported by MCFs and limited by ICXT [9]. The ICXT depends on several MCFs parameters and characteristics and some strategies to suppress and mitigate its impact on the transmission can be developed after an exhaustive study of its impact on the performance [4], [10].

1.2 Objectives

This dissertation aims to study the transmission of PAM4 signals in intra-datacenters connections with optical direct-detection and homogeneous weakly-coupled MCFs, which are limited by ICXT. The dual polarization discrete changes model (DCM) is considered to characterize the ICXT induced by the cores of the MCF. To study the ICXT impact on the performance, several metrics are used: average bit-error-rate (BER), eye-pattern analysis, power penalty due to ICXT and OP. The results are obtained by numerical simulation in Matlab. The main objectives of this work are:

• Characterization and implementation of short-haul optical telecommunication systems with direct-detection and PAM4 modulation formats transmission;

• Study and implementation of the dual polarization DCM to characterize the ICXT in weakly-coupled homogeneous MCFs;

• Evaluation of the impact of ICXT in direct-detection communication systems with PAM4 signal transmission supported by weakly-coupled homogeneous MCFs,

through several performance metrics: average BER, eye-pattern analysis, power penalty and OP;

- Compare the PAM4 modulation tolerance to ICXT with the OOK modulation tolerance.

1.3 Dissertation organization

This work has the following structure. In chapter 2, the most important concepts related to transmission of PAM4 signals in datacenters connections and MCFs are described. More specifically, concepts related to the evolution of the datacenter architecture and the transmission in datacenters connections, and the use of MCFs to support the datacenters transmission are presented. In chapter 3, the optical telecommunication equivalent system model to study the impact of ICXT in short direct-detection links with PAM4 transmission is presented, namely: the optical transmitter and the generated PAM4 signal, the dual polarization DCM, that models the ICXT on the MCF, and the optical direct-detection receiver. Also in this chapter, the validation of the equivalent system model is performed through the evaluation of the BER. In chapter 4, the impact of the ICXT on the transmission of PAM4 signals in intra-datacenters connections is assessed with a special emphasis on the OP metric. Particularly, the OP studies are performed for a different number of interfering cores, high and low fiber dispersion and considering the time misalignment between signals in the different fiber cores. The power penalty due to ICXT and the OP of the system are studied and compared. Finally, in chapter 5, the final conclusions are presented.

1.4 Main original contributions

This work presents the following main original contributions:

• Proposal of PAM4 transmission supported by MCFs in intra-datacenters connections to cope with 100 Gb/s transmission per channel;

• Implementation of a combined technique of simulation and theoretical analysis to assess the performance of PAM4 systems with direct-detection supported by MCFs and impaired by ICXT;

• Analysis of the effect of the ICXT on the eye-patterns, for different skew-symbol rate products and several extinction ratios;

• For the first time, assessment of the power penalty and OP in PAM4 systems with direct-detection limited by ICXT with one interfering core;

• Demonstration that the PAM4 signal is much less tolerant to ICXT than OOK modulation;

• Evaluation of the OP in PAM4 systems with direct-detection with ICXT originated in several interfering cores;

• Assessment of the influence of the time misalignment between the signals in the different cores on the OP for PAM4 systems;

• Conclusion that the OP is a very important metric to analyze the ICXT impact on PAM4 systems and guarantee the quality of service in such systems.

Chapter 2

Fundamental concepts

This chapter will present some literature review with an emphasis in the most important concepts related to this work. In sections 2.1 and 2.2, a review of the state-of-the art concerning the evolution of the transmission between data-centers using optical communications system is presented. Section 2.3 provides some general concepts regarding optical fibers, and in section 2.4, a more deeper description on MCFs is presented. Section 2.5 makes a brief description of the ICXT impairment in MCFs and section 2.6 presents a review of several works that have proposed and studied the transmission of PAM4 signals in MCFs.

2.1 Datacenters architecture evolution

The evolution of technology has led to the creation of datacenters that provide economically viable and flexible access to the necessary resources and storage, taking into account the current needs of Internet data services. Datacenters are buildings intended for housing a large number of servers connected to a large data network and associated components, managed by an operator. In addition to computer systems and to ensure their safety, are also part of the datacenter, power supplies that ensure backup power, communication equipment and cabling systems, air conditioning, fire suppression and security devices [11].

In recent years, datacenters have been increasingly used by large Internet service providers to store and process large amounts of information and have an important role in information technology, providing and storaging communications and network services to the growing number of networked users and devices. This led to the development of hyperscale datacenters, which are large-scale public cloud datacenters [1]. Fig. 2.1 shows the global hyperscale datacenter growth. From 2016 to 2021, the number of hyperscale datacenters is expected to increase from 338 to 628, and by 2021 will represent 53 % of all installed datacenters [1].

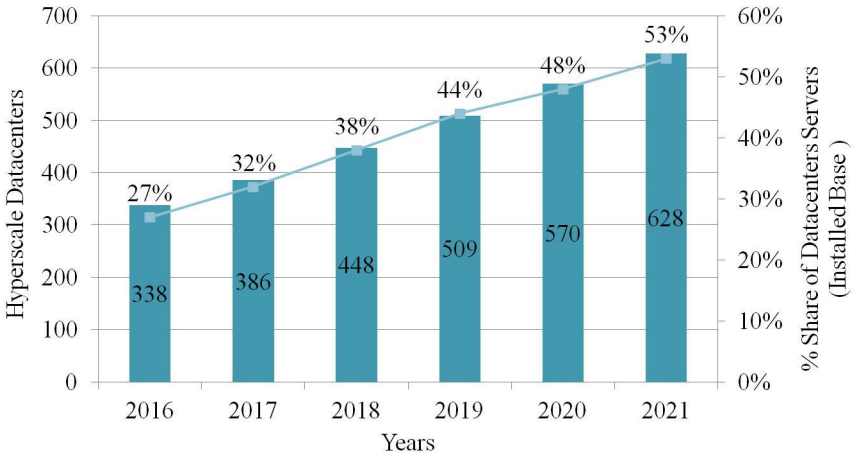

FIGURE 2.1: Global hyperscale datacenter growth [1].

As the number of datacenters has increased in recent years, so has the traffic between them. That is, traffic from the datacenter to the user, where traffic flows from the datacenter to the user over the Internet or Wide Area Networks (WANs); datacenter to datacenter traffic where traffic flows from one datacenter to another; and within datacenter refers to traffic that circulates within the datacenter. Fig. 2.2 shows the expected global growth of traffic in datacenters from 2016 to 2021. In case of traffic within datacenters, it is expected a growth from 5143, in 2016, to 14695 Exabyte (EB) per year in 2021, which represents an increase of 23.4 % of the compound annual growth rate (CAGR). Datacenter to datacenter traffic is expected to increase from 679 to 2796 EB per year, which represents a 32.7 % CAGR. Datacenter to use traffic will increase 25.2 % CAGR, from 998 to 3064 EB per year [1].

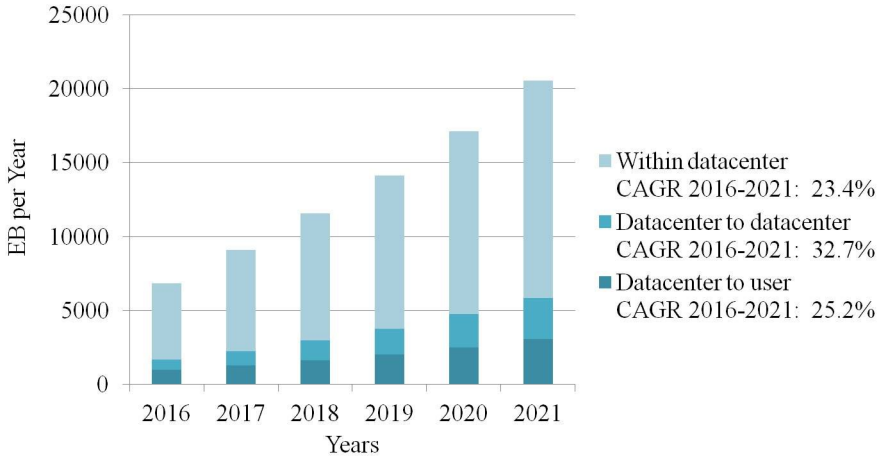

FIGURE 2.2: Global datacenter traffic [1].

When a request is made by an user, the packet is routed through the Internet to the front end of the datacenter and then to the appropriate server [12]. Thus, large volumes of data are generated, which has led to the requirement for the datacenters expansion. [1]. With the exponential growth of required capacity in datacenters, traffic, which was mainly transmitted only between external datacenters to servers, data traffic started to be transfered between servers inside the same datacenter or anothers nearby.

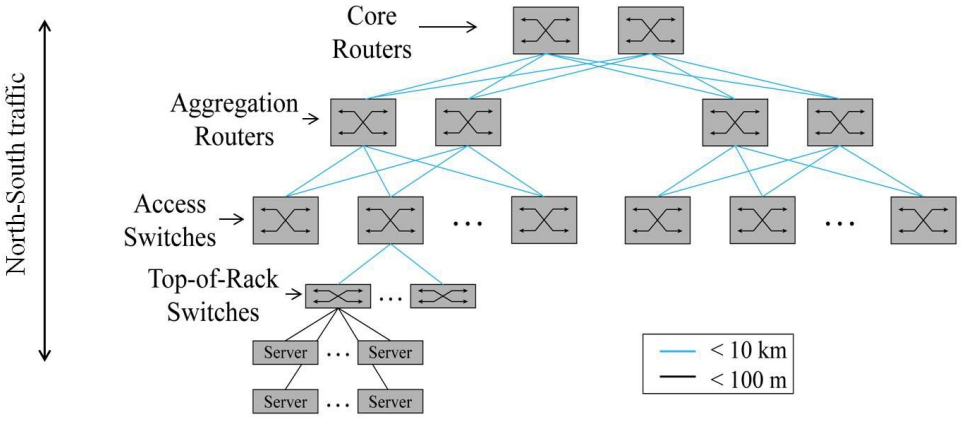

FIGURE 2.3: Traditional datacenter architecture with 3 layers: access switches, aggregation routers and core routers. The connections links with different distances are also depicted.

A traditional datacenter which has an architecture with three layers, is shown in Fig. 2.3, where servers, through Top-of-Rack switches (ToR), are connected to access switches that, in turn, connect each one to two aggregation routers for redundancy and finally, these routers are connected to the core routers with

redundancy. This architecture is efficient to manage north-south traffic, which is the traffic to the user, but is not enough to manage east-west traffic, which is the traffic within datacenter and between datacenters [1]. The traffic between servers in the same datacenter has to travel to the core layer and then back through the access switches, two aggregation routers and the core router of the other datacenter [3], [12]. The distance between servers ans servers and ToR is about 100 km and the links between the layers in this architecture have a length of typically 10 km.

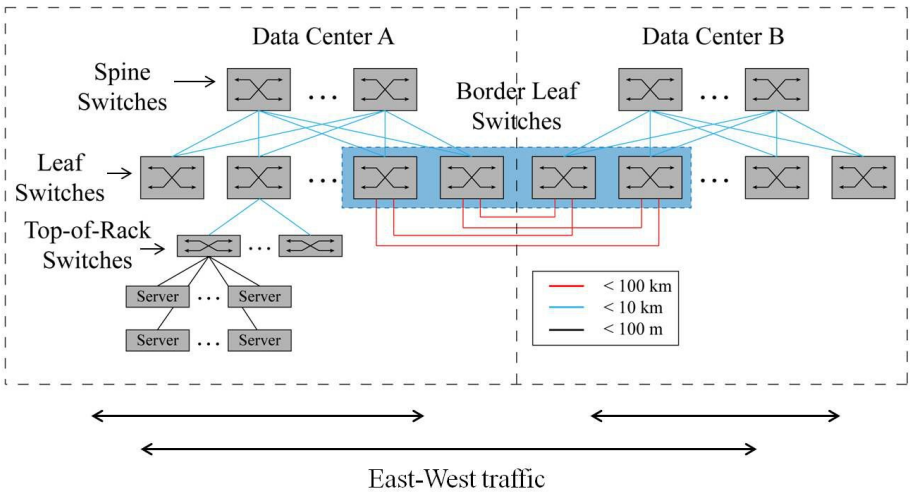

FIGURE 2.4: "Two-tier" datacenter architecture with 2 layers: leaf switches and spine switches. The connections links with different distances are also depicted.

To overcome this issue, traditional datacenter architectures have evolved into a "two-tier" architecture, as illustrated in Fig. 2.4. In this architecture, servers are connected to ToR switches that are connected to leaf switches, which in turn are connected to all spine switches, resulting in a high number of paths inside the datacenter. East-west traffic travel to a spine switch before traveling to the desired leaf switch, that is, the leaf swtiches do not communicate with each other, which results in low latency. The network is easily expandable by adding leaf switches or spine switches as needed. This architecture also improves resilience to failures, since the failure of a spine switch only results in a small decrease in performance. The connection between neighboring datacenters, with a distance of less than 100 km, which is classified as an inter-datacenter connection, is ensured through the connection between their borders leaf switches [3]. The transmission between and inside datacenters is mainly supported by optical fibers.

2.2 Signal transmission in datacenters connections

The current solution to increase capacity and scale the connections of the datacenters is the use of multiple fibers to carry WDM channels, each channel composed by an OOK signal. OOK is the simplest modulation format, however it leads to the lowest channel capacity due to it is lower spectral efficiency [3]. The PAM4 has been studied [9], [13] for several short-haul optical interfaces motivated by the need to maintain the low cost structure of these interfaces and to allow the use of lower cost optical components. It is a solution that allows to increase the link capacity through the use of higher spectral efficiency than the OOK [14], [15]. The PAM4 modulation format is characterized by four amplitude levels, representing a symbol, where each symbol is generated by the combination of two bits. By transmitting two bits in a symbol period, the PAM4 reduces the bandwidth of the signal by half, and doubles the spectral efficiency. Hence, this format encodes data in the amplitude of a sequence of signal pulses, and is expected to be an economical and efficient 100G and 400G enabler in intra and inter-datacenter connections [3], [14]. Thus, PAM4 transmission has been appointed for long and short-haul optical interfaces. In [15], the transmission in datacenters interconnects longer than 100 km, which require optical amplification and control of impairments such as chromatic dispersion, optical filtering, and amplified spontaneous emission (ASE), is assessed. In [9] and [13], the 56 Gbaud PAM4 transmission over 2 km and 2.5 km, respectively, for intra-datacenters transmission is investigated. A PAM4 transmission over 10 km and 168 Gb/s for intra-datacenters is studied in [16]. The performance of the PAM4 signal in relation to received power and range has been evaluated, and it has been concluded that up to 176 Gb/s bit rate can be transmitted over 10 km with a target BER of 4×10^{-4} and a received signal power of 8 dBm.

Datacenter connections can be classified in two types: intra-datacenter links, that appear in the architecture shown in Fig. 2.3, and inter-datacenter links, which appear in the architecture shown in Fig. 2.4 [3]. Fig 2.5 shows the system model for an intra-datacenter link, which is characterized by having a range up to 10 km

and typically operates at a wavelength near 1310 nm, to minimize total chromatic dispersion (CD). These links are usually unamplified, resulting in a low power margin [3], [17]. CD is a limitation of the fiber material related to the wavelength dependence of the refractive index of a material. Since these links are typically unamplified, avalanche photodiodes, instead of PIN photodetectors, can be used to increase the receiver sensitivity [3].

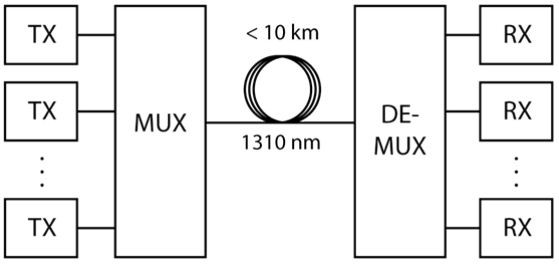

FIGURE 2.5: Intra-datacenter links. TX: transmitter, MUX: multiplexer, DE-MUX: demultiplexer, RX: receiver.

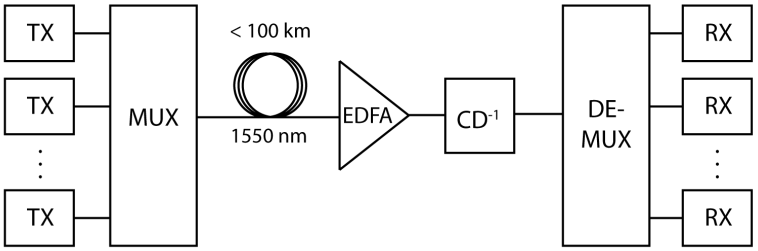

FIGURE 2.6: Inter-datacenter links. TX: transmitter, MUX: multiplexer, EDFA: erbium-doped fiber amplifier, CD^{-1}: chromatic dispersion compensation, DEMUX: de-multiplexer, RX: receiver.

Fig. 2.6 shows a schematic system model for an inter-datacenter link, which is characterized by having a range up to 100 km and uses erbium-doped fiber amplifiers (EDFAs) that operate at a wavelength near 1550 nm to amplify the signal. Accumulated CD must be compensated by dispersion shifted fibers (DSFs) or tunable fiber Bragg gratings, since CD becomes significant for these distance ranges [3], [17]. Intra and inter-datacenters communication systems use typically intensity modulation at the transmitter and direct-detection at the receiver, to ensure lower cost, which consequently leads to the dominance of amplitude modulation, such as OOK, in such systems [3].

Intra and inter-datacenters links have design priorities such as cost, power consumption, port density, and small propagation problems when compared to long-haul systems since non-linear effects are usually insignificant at these small propagation distances [3].

2.3 Optical fibers

As already mentioned in section 2.1, the transmission between and inside data-centers is supported by optical fibers. An optical fiber is a medium made by silica with low loss that allows light transmission in very long distances and with a very large available signal bandwidth. It is composed by a core with a refractive index higher than the cladding, which allows total internal reflection of light inside the core and, thus, the transmission of light along the fiber [18].

Standard optical fibers can be classified in two types: singlemode fiber (SMF) and multimode fiber (MMF). These fibers are composed by a central core composed by silica which is doped and that provides a light guiding region, confined mainly to the core. SMF is the most common fiber whose core diameter is tipically between 8 and 10 μm [19]. MMF has a larger core with a diameter of about 50 μm with a higher density of doping material and several modes of propagation are transmitted inside the core. However, the different modes have different propagation velocities, which is translated in the effect of intermodal dispersion, which limits the bit rate to a maximum of about 40 or 100 Gb/s of a digital signal that can be transmitted in MMFs [20]. For both bit rates, in case of OM3 fiber type, the link distance is usually 100 m, and for OM4 type, the link distance is 150 m. As SMFs have only one mode inside the core, intermodal dispersion is inexistent. SMF are the most deployed fibers [21] and can achieve very high bit rates, about 100 Tb/s in very long distances. In this work, only single-mode propagation will be considered.

The performance of the optical fiber as a data transmission channel can be limited by several effects, such as attenuation, dispersion and non-linear effects. The attenuation is caused by the Rayleigh scattering and the material absorption.

The Rayleigh scattering depends on the wavelength and varies with a dependence on λ^{-4}. The material absorption can be intrinsic, which is caused by the absorption of the silica, or extrinsic, which is caused by impurities of the silica [18]. A typical fiber attenuation is 0.2 dB/km, for a wavelength near 1550 nm, and 0.5 dB/km for 1310 nm [18].

There are two type of dispersion in SMFs: chromatic dispersion and polarization-mode dispersion (PMD). The chromatic dispersion is due to the contributions of material dispersion and waveguide dispersion. The material dispersion is caused by a change in the refractive index of the silica with the wavelength. The waveguide dispersion depends on the waveguide material. The waveguide material depends on fiber parameters, such as the core diameter and the index difference. It is possible to design the fiber, so, that the zero-dispersion wavelength is shifted to 1550 nm. These fibers are called DSFs [18]. The PMD results from the birefringence of the fiber that varies along the fiber lenght and causes the optical pulses to be enlarged. Birefringence occurs due to the different refractive indices of the degenerated modes that propagated along the fiber [18].

The non-linear effects are caused by the response of the dielectric to light that can modify the properties of the medium and produce a non-linear behaviour. The non-linear effects are generated by the Kerr effect and the inelastic scattering [18], [22]. The Kerr effect occurs when the light intensity on the fiber influences the refractive index. This effect originates self-phase modulation (SPM), cross-phase modulation (XPM) and four-wave mixing (FWM). The SPM produces chirp on the optical pulses and, in conjunction with CD, leads to an increase of the intersymbol interference (ISI) at the receiver. The XPM comes from the same process as SPM, but with a second wave, propagating inside the fiber, as in a WDM system. In FWM, the interaction of two or three incident light waves originates additional wavelengths that create interference, when they mix with the wavelengths already existing inside the fiber [22]. Finally, the inelastic scattering results from the stimulated Raman scattering (SRS) and the stimulated Brillouin scattering (SBS), where, the main difference between them is that, SRS is related with optical waves, while, SBS is related with acoustic waves [18], [22].

2.4 Multicore fibers

The transmission in datacenters is mainly done through the use of SC-SMF [5]. Recent SC-SMF transmissions have achieved a transmission capacity of about 100 Tb/s and a capacity-distance product over 100 Pb/s·km for a distance of 8000 km. However, it is expected that this maximum transmission capacity cannot meet the expected future volume of Internet traffic and can lead to a capacity crunch [4]. This problem can be solved through the use of space division multiplexing (SDM). SDM consists of incorporating multiple independent transmission channels into a fiber. These channels can correspond to different modes in case of the few-mode fibers (FMF) or to individual cores in the case of MCFs [6]. MCFs are one of the most attractive technologies to overcome the capacity limits attainable with SC-SMF [4]. Recent transmissions with MCF have reached capacities of 10 Pbps·km for a distance of 1000 km or up to 1 Ebps·km for 8000 km, which is ten times more than the capacity of MCFs for 8000 km [4].

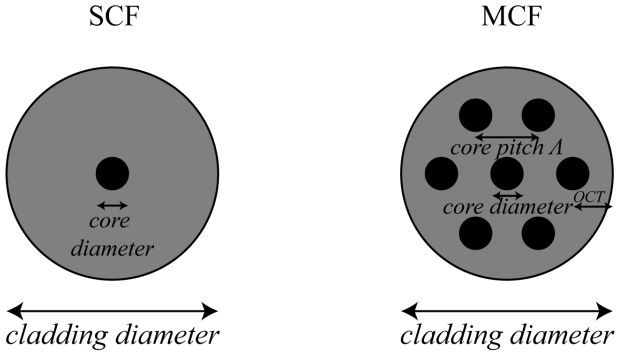

FIGURE 2.7: Cross section of a single-core fiber (SCF) and a 7-core MCF.

MCFs can have between 2 and 31 cores depending on the core diameter, the core pitch, which is the core-to-core distance, and the outer cladding thickness (OCT), that is the minimum distance between the center of the outer cores and the cladding-coating interface [21]. Fig. 2.7 shows the cross section of a SCF and of a MCF, where it is possible to see the several cores inside the cladding of the MCF and where several parameters of the fibers such as core diameter, cladding diameter, core pitch and OCT are schematically presented. These parameters vary accordingly to the type of fiber. In SCF, the core diameter is about 9 μm and the

cladding diameter is about 125 μm. In MCFs, the core diameter is about [8.6;9.5] μm, and the cladding diameter can vary between 200 μm and 300 μm depending on the number of cores [21]. The core pitch, depends on the type of MCF, may be below or above 30 μm, and the OCT is usually 20 μm [4], [23].

MCFs can be classified in two categories regarding the coupling between the cores: weakly-coupled multicore fiber and strongly-coupled multicore fiber [4]. In weakly-coupled MCFs, the core pitch is higher than 30 μm, the coupling coefficient is lower than 0.01 m^{-1} and each core can work as an individual waveguide with low level of interference between neighboring cores [4]. The signal interference due to the coupling between cores is called ICXT. In strongly coupled MCFs, the core pitch is lower than 30 μm, the coupling coefficient is higher than 0.1 m^{-1} and the ICXT is intentionally introduced by decreasing the core pitch, which results in a high level of interference between neighboring cores, but increases the core density and fiber capacity. This type of fiber needs multiple-in multiple-output (MIMO) in the digital signal processing (DSP) block at the receiver to process and reduce the ICXT. Hence, in the receiver electrical part to recover the signal, an enhanced complexity is demanded in strongly-coupled MCFs [4].

The MCFs may also be classified as homogeneous, quasi-homogeneous or heterogeneous. In homogeneous MCFs, each core has similar properties, as geometry and refractive index, and all the cores have the same propagation constant [6], [7]. Quasi-homogeneous fibers result from variations in the structure of the fiber during the fabrication process which, in turn, cause slight variations in the propagation constants of the several cores and, thus, the fiber cores are not perfectly homogeneous [7], [24]. In heterogeneous fibers, each core has a different geometry and effective refractive index, leading to different propagation constants between cores, and demands the use of DSP at the receiver to recover the signal transmitted along each core, and, therefore, the receiver is more complex to implement than in homogeneous fibers [6].

In this work, homogeneous weakly-coupled MCFs for the datacenters connections will be considered due to their lower complexity at the receiver. However,

homogeneous MCFs lead to ICXT, which may limit significantly the short-haul direct-detection datacenters connections performance or the link reach [6].

2.5 ICXT in MCFs

The existence of parallel cores in MCFs causes some coupling between cores, known as ICXT, which results from overlapping fields inside or outside the fiber, fiber imperfections and external perturbations. The ICXT is a stochastic process that has a random time varying frequency dependence which can cause some random high levels of ICXT in a short period of time [8], [25]. This high levels of ICXT can cause the system shutdown or long time periods of outage and a random fluctuation of the Q-factor. To describe the random evolution of ICXT over the time, a theoretical model, known as DCM, has been proposed, which considers single and dual polarization signals. The theoretical model is based on a time varying random phase shifts (RPSs) associated with each phase matching point (PMP) of a homogeneous MCF to describe the frequency modulation and random time nature of ICXT. The PMPs appear randomly along the fiber and the total crosstalk is approximated by the sum of the contributions of PMPs weighted by the RPSs and corresponding propagation delay [26]. This work is based on the dual polarization DCM with two cores to characterize the ICXT induced by the cores of the MCF. This model is detailed in chapter 3.

The ICXT affects the signal quality and, for that, its characterization and suppression has been intensively studied over the years. Previous works have shown that the ICXT has a high dependence on MCFs parameters and wavelength. In [10], a low crosstalk and low loss MCF was designed and fabricated based on the dependence of the ICXT of the fiber bend. In [9], the impact of ICXT on a 56-Gbaud PAM4 transmission over 2.5 km 7-core fiber is studied, and, concludes that, the ICXT is also dependent on the wavelength. The results show that longer wavelengths are more affected by ICXT.

Thus, in order to suppress the ICXT impact, there are some strategies that can be followed [6]. One of the strategies for decreasing the ICXT in MCFs, is to reduce the coupling coefficient between cores. As such, trench-assisted MCFs and hole-assisted MCFs have been proposed as a solution [4]. Due to the existence of low index trench layers, the overlap of the electromagnetic fields between the cores can be greatly suppressed, resulting in enhanced crosstalk suppression. Another option, to reduce crosstalk, is the use of heterogeneous MCFs, since all the cores have a different propagation constant, which reduces the coupling. Other way, to suppress crosstalk in MCFs, is to use the propagation-direction interleaving (PDI) technique. In this technique, the adjacent cores are assigned in opposite transmission directions to reduce the number of adjacent cores in which the signal propagates in the same direction and, thus, mitigating the crosstalk effect [4].

2.6 PAM4 signals transmission over MCFs

In the last few years, the PAM4 format has been proposed and studied for signals transmission on MCFs in short-haul links, being the main goal to upgrade the capacity. In [13], a 400 Gb/s transmission over a single-wavelength and single-MCF is achieved experimentally using a 4-core MCF with 125 μm, a core pitch of 44.8 μm at λ=1310 nm over 2 km. Furthermore, a 1.6 Tb/s transmission using 56 Gbaud PAM4 over 2 km is achieved using the same fiber now at λ=1550 nm using coarse WDM over the C+L band. The aim of these experiments is to demonstrate the transmission of such high cpacities in MCFs over distances typical of local area networks using MCFs instead of parallel SC-SMFs. In [27], a 56 Gbit/s PAM4 signal is transmitted over 15 km and a 84 Gbit/s PAM4 over 1 km SSMF, using a low power, low cost and long wavelength vertical cavity surface emitting lasers VCSEL (1525 nm). The results achieved shown that PAM4 combination with a VCSEL is an interest solution for short-reach transmissions. In [9], the impact of ICXT in MCFs on 56 Gbaud PAM4 signal along transmission 2.5 km over a weakly-coupled and uncoupled 7-core fibers is studied, and it is concluded that the ICXT depend on carrier wavelength in the range of 1540-1560 nm. Longer

wavelengths leads to a worse transmission performance which cause a higher instability in systems with weakly-coupled MCFs. In [28], the transmission of PAM4 signals is demonstrated over 10 km MCFs using directly modulated lasers, instead of external modulation as used in [13], at more modest bit rate, 10 and 20 Gb/s. Regarding the characteristics and type of the MCF, no much information is provided. The aim of the experiment is to demonstrate the transmission of PAM4 over MCFs using a cheaper transmitter configuration based on direct-modulation. In [5], the application of MCFs in short-reach systems demanding high capacity volume, such as inter-datacenters connections (with less than 2 km) is discussed thoroughly for the first time. There, it is forecast that such short-reach systems can be the first high volume application of MCFs, since most technical challenges have been tackled, especially, there is no need to address the challenge of MCF optical amplification. In that work, 200 m and 2 km MCF successful error free transmission has been achieved. In [29], an experiment with 1.04 Tb/s aggregate capacity and 80 Gbaud PAM4 per WDM channel per core over a 7-core MCF with 1 km has been reported. In this case, the MCF used is a low crosstalk fiber with a core pitch of 42 μm and crosstalk between adjacent cores of -45 dB/100 km with low loss fan-in/fan-out devices. The downside of this experiment is the very high symbol rate used, which demands very large optical and electrical components and surpasses broadly the 50 Gbaud state-of-the-art bandwidth.

Chapter 3

System model description and performance assessment

In this chapter, the optical telecommunication equivalent system model under study is presented in section 3.1. The optical transmitter is presented in section 3.2 with an emphasis on the PAM4 signal generation description. The dual polarization DCM of the MCF, which is used to generate the ICXT, is explained in section 3.3. In section 3.4, the direct-detection optical receiver model is presented. The method used to perform the BER calculation is described in section 3.5, and the validation of the BER estimation is performed in section 3.6.

3.1 System model

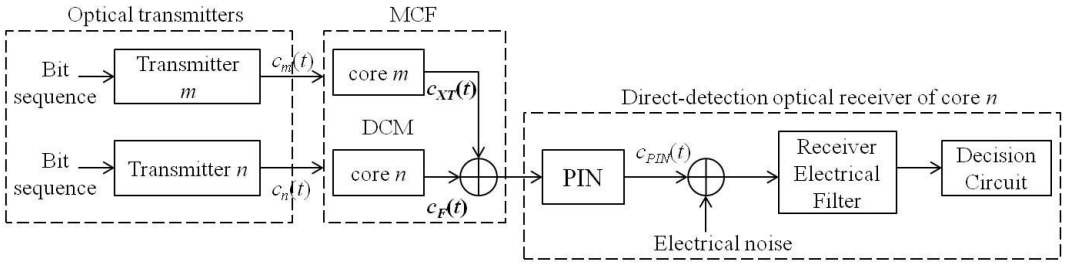

FIGURE 3.1: Equivalent system model.

The equivalent model of the intra-datacenter link supported by MCFs with PAM4 signal generation at the transmitter considered in this work is shown in Fig. 3.1. It is composed by two optical transmitters, with $c_m(t)$ and $c_n(t)$ being the PAM4 signals at the output of each transmitter. Then, a representation of the MCF that considers an interfered core n and a single core of interference m, and that the signals are transmitted in the two polarization directions **x** and **y** inside the MCF is depicted in Fig. 3.1. The signal $c_{XT}(t)$ represents the signal core m that induces ICXT on the signal in core n and interferes with the signal at the output of core n, $c_F(t)$. Fig. 3.1 shows also the direct-detection optical receiver that includes the PIN photodetector, where $c_{PIN}(t)$ is the signal at the output of the PIN photodetector, electrical noise addition, electrical filtering and the decision circuit to estimate the BER. Each one of these components is described with more detail in the following subsections.

3.2 Optical transmitter

The optical transmitters considered in this work convert the bits sequence generated from the electrical domain to the optical domain, without distortion and taking into account the signal extinction ratio. Two transmitters, one for the interfering core and the other for the interfered core, each one generating a different PAM4 signal are considered. An ideal linearized model without chirp for each optical transmitter is assumed.

The PAM4 modulation format maps two bits in each symbol, which reduces the bandwidth requirement by half when compared to OOK signals [30]. In the simulator, the converted symbols optical sequence is generated using deBruijn sequences obtained from Galois arithmetic of maximum length 4^{N_b}, where N_b represents the length of the offset register used to generate the sequence. In this way, a deBruijn sequence is generated where the symbols $'0'$, $'1'$, $'2'$ and $'3'$ are equally likely to occur [31].

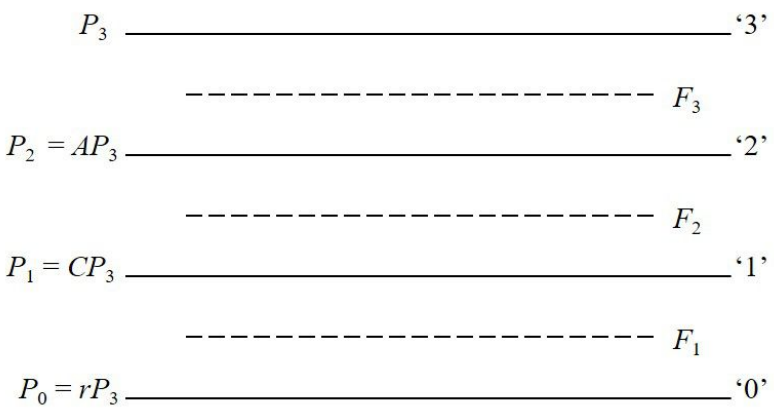

FIGURE 3.2: Representation of the power levels of an optical PAM4 signal with non-zero extinction ratio and the corresponding decision thresholds.

Fig. 3.2 shows a representation of the PAM4 signal power levels assuming a non-zero extinction ratio where $'0'$, $'1'$, $'2'$ and $'3'$ represent the symbols of the PAM4 signal; F_1, F_2 and F_3, are the ideal decision thresholds; P_3, P_2, P_1 and P_0 are the powers corresponding to each of the symbols, and r represents the extinction ratio defined as in [32]

$$r = \frac{P_0}{P_3} \tag{3.1}$$

Eq. 3.1 corresponds to the inverse of the definition of the extinction ratio as defined by ITU-T [19]. The constants A and C define the spacing between the intermediate levels of the PAM4 signal [32]. For equidistant levels, A and C are given, respectively, by [32]

$$A = \frac{2}{3} + \frac{1}{3}r \tag{3.2}$$

$$C = \frac{1}{3} + \frac{2}{3}r \tag{3.3}$$

The average power of the PAM4 optical signal is then given by [32]

$$\overline{P_{av}} = \frac{1 + A + C + r}{4} P_3 \tag{3.4}$$

After generation, the ideal PAM4 signal is filtered by a 3^{rd} order Bessel filter, in order to introduce some amplitude distortion and have a more realistic signal shape at the MCF input. The -3 dB bandwidth of the Bessel filter is defined as

$B = R_s$, where R_s is the symbol rate. The eye-pattern at the output of the optical transmitter is shown in Fig. 3.3 a) and b), respectively, for $r = 0$ and $r = 0.1$, where it can be observed that there is no ISI on the transmitted symbols at the optimum sampling instants. These eye-patterns represent the PAM4 transmitted signals $c_n(t)$ and $c_m(t)$ shown in Fig. 3.1.

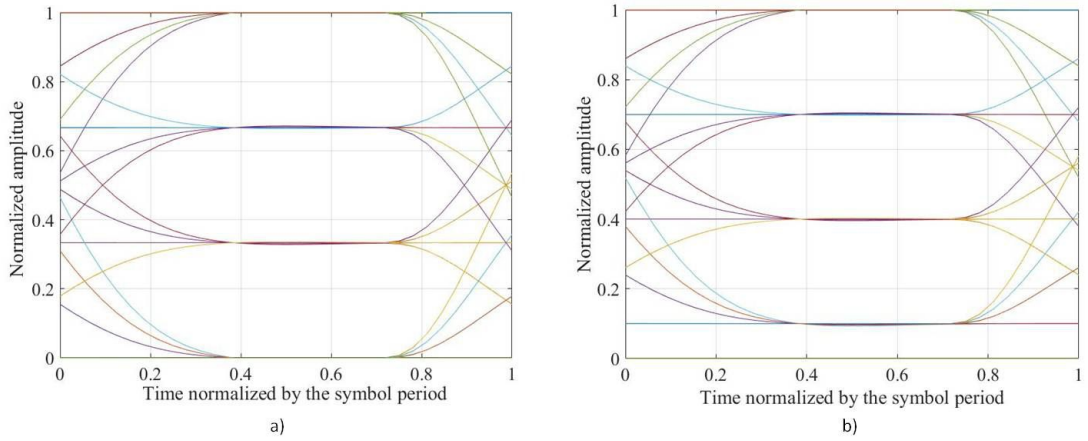

FIGURE 3.3: Normalized eye-pattern at the MCF input, after filtering by a 3^{rd} order Bessel filter with bandwidth of 56 GHz, for a) $r = 0$ and b) $r = 0.1$.

3.3 Multicore fiber modelling

To characterize the ICXT induced by the cores of the MCF, the dual polarization DCM with two cores is considered [33]. Linear propagation along the MCF is assumed in the two cores, where m and n are the interfering and interfered cores, respectively. The signal at the input of core m, $c_m(t)$, is the interfering PAM4 signal and the signal at the input of core n, $c_n(t)$, is the interfered PAM4 signal.

3.3.1 Dual polarization DCM

The dual polarization MCF DCM model considers that the optical signal is transmitted in the two polarizations directions $\mathbf{x}$ and $\mathbf{y}$, i.e, a power splitting of the transmitted PAM4 signal by the polarization directions $\mathbf{x}$ and $\mathbf{y}$ is made at the input of the MCF, as shown in Fig. 3.4 [33]. For core m, this power splitting is

represented as

$$c_{m,x}(t) = c_m(t) \times \sqrt{\xi_m}$$
$$c_{m,y}(t) = c_m(t) \times \sqrt{1 - \xi_m} \tag{3.5}$$

where $c_{m,x}(t)$ corresponds to the PAM4 signal in polarization $\mathbf{x}$, $c_{m,y}(t)$ corresponds to the PAM4 signal in polarization $\mathbf{y}$ and ξ_m controls the power distribution in both polarization directions. The parameter ξ_m can vary between 0 and 1 [33].

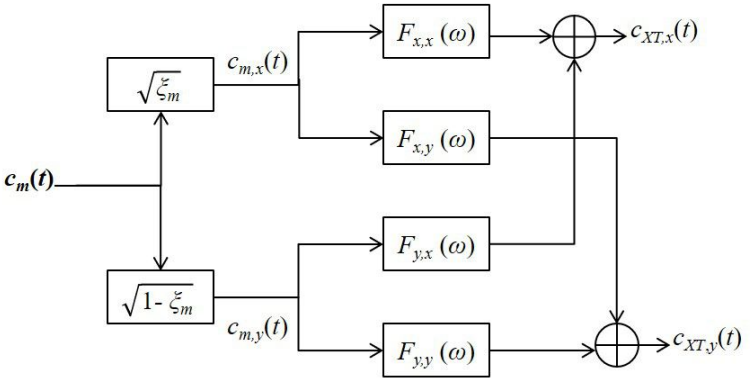

FIGURE 3.4: Dual polarization discrete changes model [33].

The transfer functions $F_{x,x}(\omega)$, $F_{x,y}(\omega)$, $F_{y,x}(\omega)$ and $F_{y,y}(\omega)$ model the ICXT from the input of core m to the output of core n and are given by [33]

$$F_{a,b}(\omega) = -\frac{j}{\sqrt{2}}\overline{K}_{nm} \exp\left[-j\overline{\beta}_n(\omega)L\right] \sum_{k=1}^{N_p} \exp\left[-j(\overline{\beta}_m - \overline{\beta}_n)z_k\right] \exp\left[-j\phi_{nm,k}^{(a,b)}\right] \tag{3.6}$$

where $a, b \in \{x, y\}$, $\overline{K}_{nm}$ is the average inter-core coupling coefficient of the polarization directions given by $\overline{K}_{nm}=(K_{nm}^{(x)} + K_{nm}^{(y)})/2$ [33]; ω is the angular frequency; L is the MCF length; $\overline{\beta}_m$ and $\overline{\beta}_n$ are the average of the propagation constants of both polarizations in cores m and n and are defined by, respectively, $\overline{\beta}_m = (\beta_m^{(x)} + \beta_m^{(y)})/2$ and $\overline{\beta}_n = (\beta_n^{(x)} + \beta_n^{(y)})/2$ [33]; z_k is a longitudinal coordinate corresponding to the k-th PMP, with N_p the number of PMPs [34]; $\phi_{nm,k}^{(a,b)}$ is a RPS associated with the k-th PMP, and is modelled by an uniform distribution between 0 and 2π. The RPSs model random variations of the bending radius, twist rate or other conditions in the MCF [33], [34]. The transfer functions $F_{x,x}(\omega)$ and $F_{y,x}(\omega)$ model the ICXT generated from polarizations $\mathbf{x}$ and $\mathbf{y}$ of core m to the polarization $\mathbf{x}$

of core n. The transfer functions $F_{x,y}(\omega)$ and $F_{y,y}(\omega)$ model the ICXT generated from both polarizations of core m to the polarization $\mathbf{y}$ of core n [33].

The signals that interfer with the signal at the output of the core n, $c_{XT,x}(t)$ and $c_{XT,y}(t)$, are given by

$$\begin{aligned} c_{XT,x}(t) &= c_{m,x}(t) * \mathcal{F}^{-1}[F_{xx}(\omega)] + c_{m,y}(t) * \mathcal{F}^{-1}[F_{yx}(\omega)] \\ c_{XT,y}(t) &= c_{m,x}(t) * \mathcal{F}^{-1}[F_{xy}(\omega)] + c_{m,y}(t) * \mathcal{F}^{-1}[F_{yy}(\omega)] \\ \mathbf{c_{XT}(t)} &= c_{XT,x}(t)\hat{\mathbf{x}} + c_{XT,y}(t)\hat{\mathbf{y}} \end{aligned} \tag{3.7}$$

where $*$ stands for convolution and $\mathcal{F}^{-1}$ stands for the inverse Fourier Transform.

The power splitting, for core n, shown in Fig. 3.1 is represented by

$$\begin{aligned} c_{n,x}(t) &= c_n(t) \times \sqrt{\xi_n} \\ c_{n,y}(t) &= c_n(t) \times \sqrt{1-\xi_n} \end{aligned} \tag{3.8}$$

where $c_{n,x}(t)$ and $c_{n,y}(t)$ are the PAM4 signal in polarizations $\mathbf{x}$ and $\mathbf{y}$ at the input of core n, respectively. The parameter ξ_n controls the power distribution in both polarization directions and can vary between 0 and 1 [33]. After the power splitting, the PAM4 signal passes through the core n of the MCF, which is modelled by the linear propagation transfer function $H_F(\omega)$ and the signal at the output of core n without ICXT is given by

$$\begin{aligned} c_{F,x}(t) &= c_{n,x}(t) * \mathcal{F}^{-1}[H_F(\omega)] \\ c_{F,y}(t) &= c_{n,y}(t) * \mathcal{F}^{-1}[H_F(\omega)] \\ \mathbf{c_F(t)} &= c_{F,x}(t)\hat{\mathbf{x}} + c_{F,y}(t)\hat{\mathbf{y}} \end{aligned} \tag{3.9}$$

where $H_F(\omega)$ is given by [18]

$$H_F(\omega) = \exp\left(-j\overline{\beta_n}(\omega)L\right) \tag{3.10}$$

The fiber attenuation is considered the same in both cores. Hence, in this work,

the level of attenuation is not relevant in our analysis and the receiver sensitivity is considered to assess the system performance.

3.4 Optical receiver

After passing through the MCF, the PAM4 signal impaired by ICXT arrives at the direct-detection optical receiver input, as shown in Fig. 3.1, which includes a PIN photodetector, an electrical filter and a decision circuit.

3.4.1 PIN photodetector

PIN photodiodes convert light into electricity through the photoelectric effect. The signal at the output of the PIN photodetector, $c_{PIN}(t)$, is given by [32]

$$\begin{aligned} c_{PIN}(t) &= R_\lambda[|c_{XT,x}(t) + c_{F,x}(t)|^2 + |c_{XT,y}(t) + c_{F,y}(t)|^2] \\ &= R_\lambda[|c_{XT,x}(t)|^2 + |c_{F,x}(t)|^2 + 2 \cdot \mathrm{Re}[c_{XT,x}(t) \cdot c_{F,x}(t)] + \\ &\qquad |c_{XT,y}(t)|^2 + |c_{F,y}(t)|^2 + 2 \cdot \mathrm{Re}[c_{XT,y}(t) \cdot c_{F,y}(t)]] \end{aligned} \quad (3.11)$$

where R_λ is the PIN responsivity given by [18]

$$R_\lambda = \frac{\eta q}{h\nu} \quad [\mathrm{A/W}] \quad (3.12)$$

where η is the photodetector efficiency, q is the electron charge (q=1.602×10^{-19} C), h is the Planck constant (h=6.602×10^{-34} J·s) and ν is the optical frequency of the incident optical power. In this work, a responsivity of R_λ=1 A/W is considered.

3.4.2 Electrical noise

The thermal noise is added to the current generated at the output of the PIN photodetector and is modeled by a Gaussian distribution. The power of the thermal

noise is given by [18]

$$\sigma_c^2 = R_\lambda^2 NEP^2 B_{e,n} \tag{3.13}$$

where NEP is the Noise Equivalent Power (NEP), defined as the the minimum optical power necessary to generate a photocurrent equal to the noise current of the photodetector [18]. In this work, we consider NEP=10^{-12} W/$\sqrt{\text{Hz}}$. The bandwidth $B_{e,n}$ is the noise equivalent bandwidth of the electrical filter of the optical receiver given by

$$B_{e,n} = \int_0^{+\infty} \left| \frac{H(f)}{H(0)} \right|^2 df \tag{3.14}$$

where $H(f)$ is the amplitude transfer function of the electrical filter.

3.4.3 Electrical filter

After passing through the photodetector, the distorted signal with ICXT and electrical noise passes through an electrical filter. The electrical filter is used to reduce the power of the electrical noise without introducing much ISI [18]. In this work, to model the electrical filter, a Bessel filter is considered, whose n-th order amplitude transfer function is given by [35]

$$|H(s)| = \frac{1}{Q_n(s)} \tag{3.15}$$

with

$$s = j \cdot \frac{2f}{f_{-3dB}} \tag{3.16}$$

where f_{-3dB} is the cutoff frequency at -3 dB of the filter and $Q_n(s)$ is the n-th order polynomial factor and can be obtained from [35]

$$|Q_{n+1}(s)| = Q_n(s) + \frac{s^2}{4n^2 - 1} Q_{n-1}(s) \tag{3.17}$$

with

$$|Q_n(s)| = s^n B_n \left(\frac{1}{s} \right) \tag{3.18}$$

where B_n is the n-th order Bessel polynomial [35].

3.5 Bit error rate - BER

The BER is calculated by the semi-analytical method known as the exhaustive Gaussian approach, which is given by [32]

$$BER = \frac{1}{4^{N_b}} \left\{ \sum_{\substack{k=1 \\ a_k=0}}^{4^{N_b}} Q\left(\frac{F_1 - i_{0,k}}{\sigma_{0,k}}\right) + \sum_{\substack{k=1 \\ a_k=1}}^{4^{N_b}} \left[Q\left(\frac{i_{1,k} - F_1}{\sigma_{1,k}}\right) + Q\left(\frac{F_2 - i_{1,k}}{\sigma_{1,k}}\right) \right] + \right.$$
$$\left. \sum_{\substack{k=1 \\ a_k=2}}^{4^{N_b}} \left[Q\left(\frac{i_{2,k} - F_2}{\sigma_{2,k}}\right) + Q\left(\frac{F_3 - i_{2,k}}{\sigma_{2,k}}\right) \right] + \sum_{\substack{k=1 \\ a_k=3}}^{4^{N_b}} Q\left(\frac{i_{3,k} - F_3}{\sigma_{3,k}}\right) \right. \quad (3.19)$$

where $i_{0,k}$, $i_{1,k}$, $i_{2,k}$ and $i_{3,k}$ correspond to the means of the currents at the input of the decision circuit for the symbols '0', '1', '2' and '3', respectively; and $\sigma_{0,k}$, $\sigma_{1,k}$, $\sigma_{2,k}$ and $\sigma_{3,k}$ correspond to the noise standard deviations of the same current for the different symbols [32]. The function $Q(x)$ is given by [36]

$$Q(x) = \int_x^\infty \frac{1}{\sqrt{2\pi}} e^{-\frac{\xi^2}{2}} d\xi \quad (3.20)$$

In the simulation, the decision thresholds F_1, F_2 and F_3 are optimized by applying the bisection method to minimize the BER [37].

By considering a PAM4 sequence with 4^{N_b} symbols implies 4^{N_b} different levels of current at 4^{N_b} sampling time instants at the decision circuit input and, in this way, 4^N different contributions to the BER, as shown in Eq. 3.19. The effect of ISI from filtering and fiber dispersion is taken into account by the waveform distortion in the eye-pattern at these 4^N sampling time instants. In Eq. 3.19, this effect is included in the mean currents $i_{0,k}$, $i_{1,k}$, $i_{2,k}$ and $i_{3,k}$. As described in [38], for OOK systems, the effect of ICXT on the interfered core, is also taken into account in these means of the currents. The effect of noise is taken into account semi-analytically in the standard deviations of the received symbols. In this case, as we consider thermal noise, $\sigma_c = \sigma_{0,k} = \sigma_{1,k} = \sigma_{2,k} = \sigma_{3,k}$.

3.6 Validation of the equivalent system model

After the description of the DCM, the validation of the model through the evaluation of the BER is presented in this section. For the system model validation without ICXT, a back-to-back (B2B) configuration, is firstly used, and then fiber dispersion is included. To validate the system without ISI and ICXT, it is necessary that the BER obtained in the simulator is in agreement with the BER obtained from the theoretical expression, obtained for a B2B configuration, null ISI and additive white Gaussian noise (AWGN) noise given by [32]

$$BER_{theo} = \frac{3}{4} Q\left(\frac{1}{3} \cdot \frac{1-r}{1+r} \cdot \frac{\overline{P}_{av}}{\sigma_c}\right) \tag{3.21}$$

where $\overline{P}_{av}$ corresponds to the receiver sensitivity in a B2B configuration.

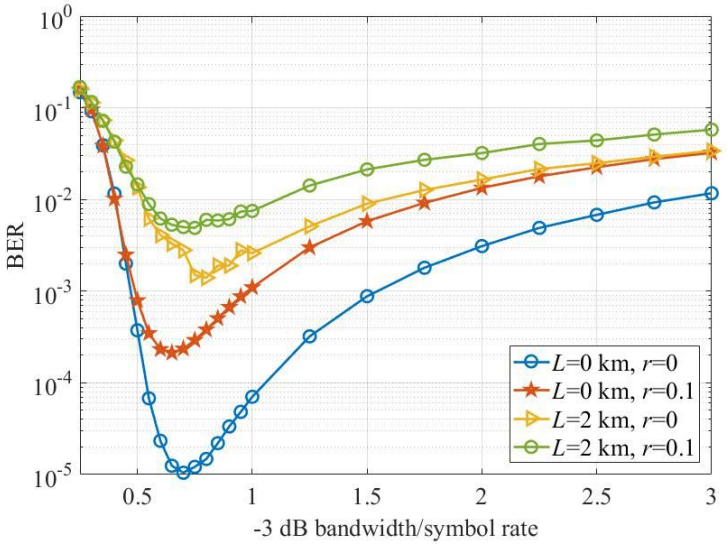

FIGURE 3.5: BER as a function of the −3 dB bandwidth of the optical receiver electrical filter normalized to the symbol rate.

Fig. 3.5 shows the variation of the BER as a function of the −3 dB bandwidth of optical receiver electrical filter, for L=0 km and L=2 km, and $r = 0$ and $r = 0.1$. For a B2B configuration, the optimum value of the electrical filter −3 dB bandwidth for $r = 0$ is about $0.7\times R_s$ and for $r = 0.1$ is $0.65\times R_s$. For L=2 km, which is the maximum distance that we are going to consider for intra-datacenter links [3], the optimum value of the electrical filter −3 dB bandwidth for $r = 0$ is about $0.8\times R_s$ and for $r = 0.1$ is around $0.75\times R_s$. Further on, throughout

this work, in subsequent simulations, by omission, we consider for the −3 dB bandwidth of the electrical filter $0.75\times R_s$. For −3 dB bandwidths below the optimum bandwidth, the effect of ISI is dominant in the BER degradation. For values larger than the optimum value, the effect of electrical noise becomes the dominant impairment.

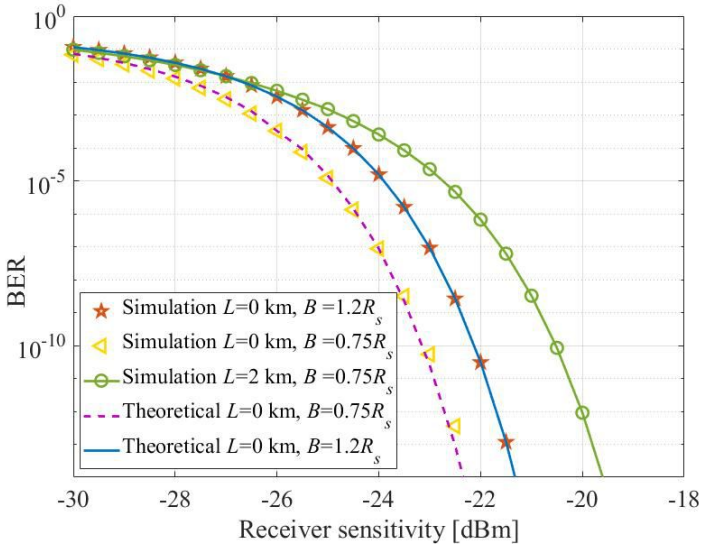

FIGURE 3.6: BER as a function of the receiver sensitivity for r=0, obtained by simulation for L=0 km and B=1.2×R_s; L=0 km and B=0.75×R_s and L=2 km and B=0.75×R_s. The theoretical BER obtained from Eq. 3.21 is also shown.

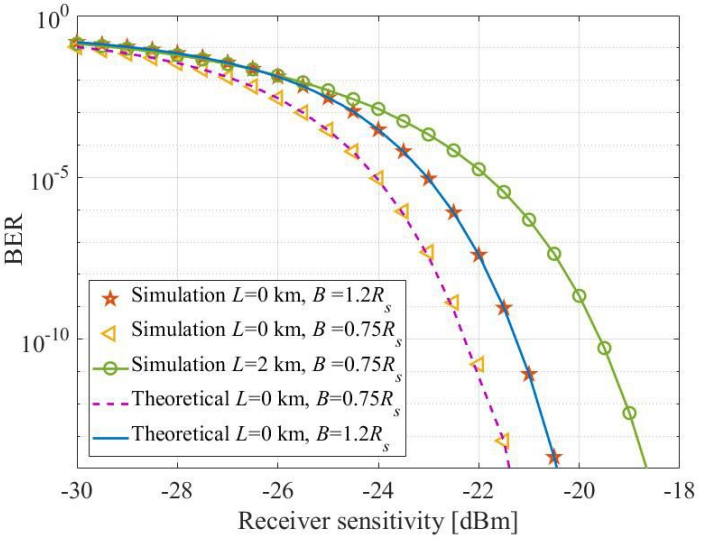

FIGURE 3.7: BER as a function of the receiver sensitivity for r=0.1, obtained by simulation for L=0 km and B=1.2×R_s; L=0 km and B=0.75×R_s and L=2 km and B=0.75×R_s. The theoretical BER obtained from Eq. 3.21 is also shown.

Figs. 3.6 and 3.7 show the theoretical and simulated BERs, for $r = 0$ and for $r = 0.1$, respectively, as a function of the receiver sensitivity for L=0 km

(B2B configuration) and L=2 km. To validate the equivalent system model and the BER method estimation, firstly, in the simulation, the Bessel filter at the transmitter was not taken into account, and in the receiver an electric filter with a bandwidth of B=1.2×R_s was considered. It can be verified that the BERs obtained by the simulator for L=0 km and B=1.2×R_s are in complete agreement with the theoretical BER, which validates the implementation of the simulator without ISI. From now on, in the simulation, it will be considered a Bessel filter at the transmitter with a bandwidth of B=1×R_s. The optimum value of the −3 dB bandwidth of receiver electrical filter B=0.75×R_s is also considered to validate the estimation of the BER through simulation, for both fiber distances, L=0 km and L=2 km, to quantify the ISI introduced from electrical filtering and fiber dispersion, respectively.

A reference target BER of 3.8×10^{-3} for directly detected PAM4 signals is assumed [39]. In the absence of ICXT, the average BER is defined two orders of magnitude below the target BER, to allow a certain margin for BER degradation due to ICXT [38] and, thus, the BER without ICXT under study that is going to be considered in this work is 3.8×10^{-5}. For the maximum fiber length considered (L=2 km), in Fig. 3.6, the optical power at the optical fiber input necessary to achieve a BER=3.8×10^{-5} is −23.2 dBm. In Fig. 3.7, to achieve a BER=3.8×10^{-5}, it is necessary an optical power at the optical fiber input of −22.3 dBm. There is a difference of about 1 dB on the receiver sensitivity from $r = 0$ to $r = 0.1$ to reach the reference BER, which corresponds to the power penalty degradation due to extinction ratio. From Eq. 3.21, the theoretical power penalty degradation due to extinction ratio is 0.9 dB, which is in agreement with the simulation results. There is also an improvement of the receiver sensitivity due to the narrowing of electrical filter bandwidth of about 1 dB, for $r = 0$, and 0.8 dB, for $r = 0.1$ since less electrical noise power reaches the decision circuit input. Also a sensitivity degradation due to the increase in fiber length, from L=0 km to L=2 km, from about 2.5 dB, for $r = 0$, and 2 dB, for $r = 0.1$ is observed.

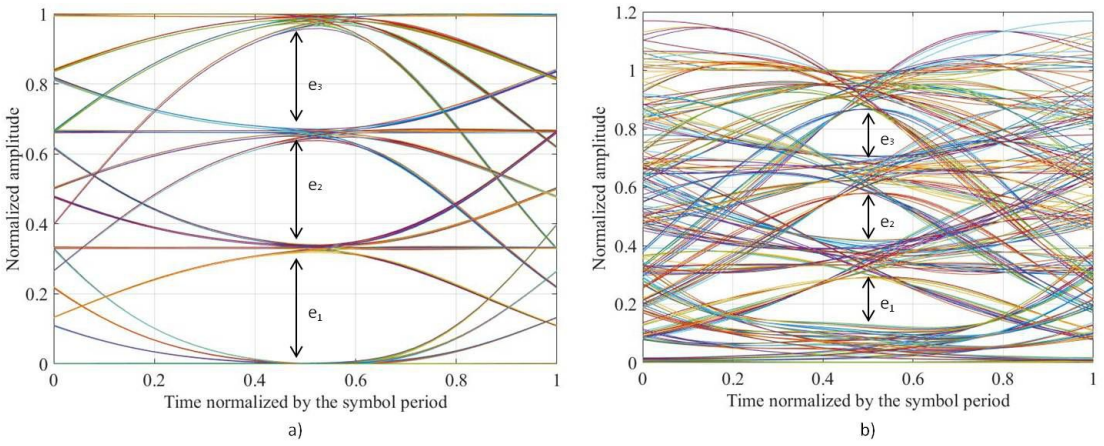

FIGURE 3.8: Eye-patterns at the decision circuit input with $r = 0$, for a) $L = 0$ km and b) $L = 2$ km.

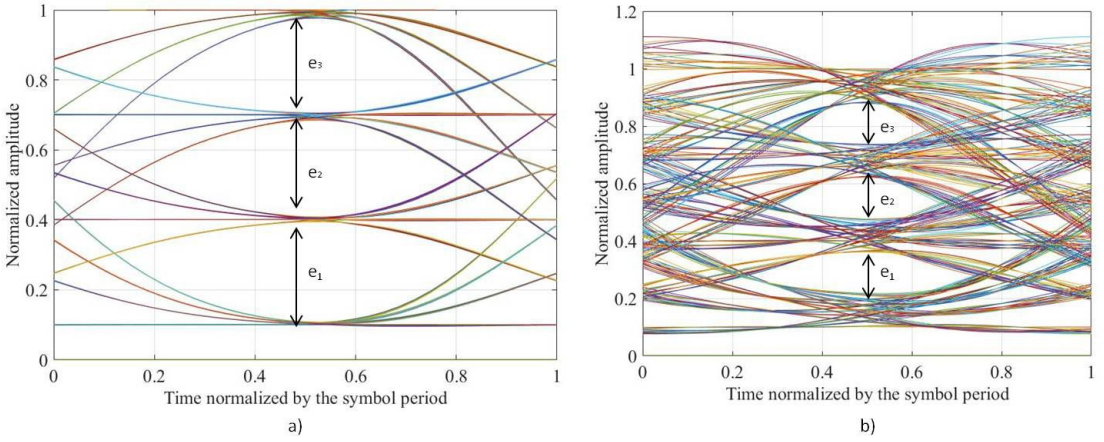

FIGURE 3.9: Eye-patterns at the decision circuit input with $r = 0.1$, for a) $L = 0$ km and b) $L = 2$ km.

The performance degradation can also be observed from the eye-patterns, through the eye closure penalty, which is associated with a corresponding increase in BER [18]. Fig. 3.8 shows the evolution of the eye-patterns at the decision circuit input for $r = 0$, where in a) the system operates in the B2B configuration (L=0 km) and b) the fiber dispersion is introduced in the system (L=2 km). Fig. 3.9 presents the eye-patterns with an extinction ratio of $r = 0.1$, for a) a B2B configuration and b) L=2 km. In Figs. 3.8 and 3.9, the power corresponding the symbol '3' is normalized to unity and the electrical filter of the optical receiver with the optimum bandwidth B=0.75×R_s is considered. It can be concluded that the performance of the system is affected by the fiber length due to the increase of dispersion, since the eye opening diminishes severely for $L = 2$ km. In Fig. 3.8 a), the normalized decision thresholds F_{n1}, F_{n2} and F_{n3} are 0.1654, 0.4936 and

0.8181 and the normalized eye openings are $e_3 = 0.3158$, $e_2 = 0.2967$, $e_1 = 0.2865$. In Fig. 3.8 b), the normalized decision thresholds are F_{n1}=0.2011, F_{n2}=0.4923 and F_{n3}=0.7893 and the normalized eye openings e_1, e_2 and e_3 are 0.1505, 0.1503 and 0.1396, respectively. In Fig. 3.9 a), the normalized decision thresholds are F_1=0.2529, F_2=0.5491 and F_3=0.8432 and the normalized eye openings e_1, e_2 and e_3 are 0.2868, 0.2765 and 0.2710, respectively. In Fig. 3.9 b), F_1, F_2 and F_3 are 0.2771, 0.5313 and 0.7836 and the normalized eye openings are $e_1 = 0.1266$, $e_2 = 0.1195$, $e_3 = 0.1223$. When comparing the normalized eye openings of Fig. 3.8 a), for $r = 0$, with Fig. 3.9 a), for $r = 0.1$, it is concluded that, for $r = 0.1$, the normalized eye openings decrease comparatively to $r = 0$ since the normalized eye height is 0.9. The same conclusion can be taken by comparing Figs. 3.8 b) and Figs. 3.9 b).

3.7 Conclusions

In this chapter, the optical telecommunication equivalent system model of the intra-datacenter optical link was presented. The optical transmitter, with an emphasis on the PAM4 signal generation, the dual polarization DCM model used to generate the ICXT and the direct-detection optical receiver composed by a PIN photodetector and an electrical filter were explained. The electrical noise at the receiver is described, and the BER estimation through the semi-analytical method exhaustive Gaussian approach is described with detail.

After presenting the equivalent system model, the BER estimated through Matlab simulation in a system with a B2B configuration and with fiber dispersion has been validated. The complete agreement between theoretical and simulated BERs validates the implementation of the simulator with and without ISI. The study of the impact of ICXT on the performance of PAM4 signals transmissions is left for chapter 4.

Chapter 4

Numerical results and discussion

In this chapter, the impact of ICXT on the performance of the transmission of PAM4 signals in short direct-detection links, emulating intra-datacenters connections, using the system model described in Chapter 3 is studied. In section 4.1, the simulation parameters are presented. In section 4.2, the pre-FEC BERs tipically used in PAM4 direct-detection systems are discussed. In section 4.3, the number of MCF realizations required to obtain a stabilized average BER is studied and the corresponding received eye-patterns are analyzed. In section 4.4, the power penalty due to ICXT is used to study the degradation caused by ICXT on the average BER, and, in section 4.5, the outage probability of the PAM4 direct-detection system is investigated in several situations: one interfering core and λ=1550 nm; one interfering core and λ=1310 nm (reduced chromatic dispersion); several interfering cores; and considering the time misalignment between signals in different cores.

4.1 Simulation parameters

To study the impact of the ICXT on the performance of PAM4 signals transmission, several metrics are used such as the average BER, power penalty and OP. The simulation parameters used throughout this chapter in these studies are presented

in Table 4.1. The number of PMPs is chosen to be high enough to characterize the RPS mechanism rigorously [34]. Two different skews, $S_{mn}{\cdot}R_s$=1000 and $S_{mn}{\cdot}R_s$=0.01 are also chosen according to the conditions $S_{mn}{\cdot}R_s \gg 1$, where the symbol rate of the PAM4 signal is much higher than the ICXT decorrelation bandwidth (which is proportional to the inverse of the skew) [40] and the ICXT creates amplitude levels that seem to exhibit a "noise" like-behavior [41], and $S_{mn}{\cdot}R_s \ll 1$, where the symbol rate of the PAM4 signal is much lower than the ICXT decorrelation bandwidth and well-defined amplitude levels in the eye-patterns are created due to ICXT [41], [40].

TABLE 4.1: Simulation parameters

Simulation parameter	Value
Symbol rate	R_s = 56 Gbaud
Number of samples per symbol	$N_s = 32$
Fiber length	L = 2 km
Number of generated PAM4 symbols in each MCF realization	$N = 4^4$
Carrier wavelength	λ = 1550 nm, 1310 nm
Fiber dispersion parameter	D_λ = 17 ps/(nm·km), 1 ps/(nm·km)
Number of PMPs	N_p = 1000
Skew-symbol rate product	$S_{mn}{\cdot}R_s$=1000, $S_{mn}{\cdot}R_s$=0.01
BER limit	$3.8{\times}10^{-3}$
BER in absence of ICXT	$3.8{\times}10^{-5}$
Number of interfering cores	N_c= 1, 2, 4
Time misalignment ratio	M= 1/8, 1/4, 3/8, 1/2, 5/8, 3/4, 7/8, 1

4.2 FEC in PAM4 systems

To use higher order modulation formats than non-return to zero (NRZ) in direct-detection optical links, forward error correction (FEC) is typically applied [39]. Table 4.2 shows the pre-FEC BERs (the BER before the DSP at the receiver,

also usually known as line BER) used in the literature in several studies of PAM4 transmission in direct-detection systems that consider FEC. In these works from Table 4.2, in a B2B configuration, the pre-FEC BER is tipically one order of magnitude lower than if there is transmission along the fiber. In this work, we consider a reference BER limit of 3.8×10^{-3}, since it is the most commonly used for intra-datacenters connections and allows more stringest transmission conditions [13], [9], [39], [42]. In this work, in absence of ICXT, the BER is defined two orders of magnitude below the target BER [38], [43], i.e, the considered BER without ICXT is 3.8×10^{-5}. To achieve this BER without ICXT, for λ=1550 nm, the receiver sensitivity is set to -23.2 dBm and -22.3 dBm, respectively, for $r = 0$ and $r = 0.1$. For λ=1310 nm, the receiver sensitivity is set to -25.3 dBm, for $r = 0$, and -24.4 dBm, for $r = 0.1$.

Notice also that the longest reach studied in the works presented in Table 4.2 is only 10 km, which is related to the application considered in our work, a short-haul direct-detection link with no amplification and absence of distortion compensation.

TABLE 4.2: Pre-FEC BER commonly used in PAM4 direct-detection systems.

Data rate	Transmission distance	pre-FEC BER	reference
56 Gbps	2, 15 km	3.8×10^{-3}	[39]
56 Gbps	B2B	5.2×10^{-4}	[39]
84 Gbps	1 km	3.8×10^{-3}	[39], [27]
84 Gbps	1.6 km	2×10^{-4}	[39]
112 Gbps	2, 4 km	3.8×10^{-3}	[13], [9], [44]
168 Gbps	B2B	2.2×10^{-4}	[42]
168 Gbps	10 km	3.8×10^{-3}	[16], [42]
336 Gbps	B2B	2.2×10^{-4}	[42]
336 Gbps	1 km	3.8×10^{-3}	[42]

4.3 Impact of ICXT on the performance of PAM4 signals transmission

The first study performed concerning the impact of ICXT on the PAM4 short-haul link performance is to assess the number of MCF realizations required to obtain a stabilized average BER.

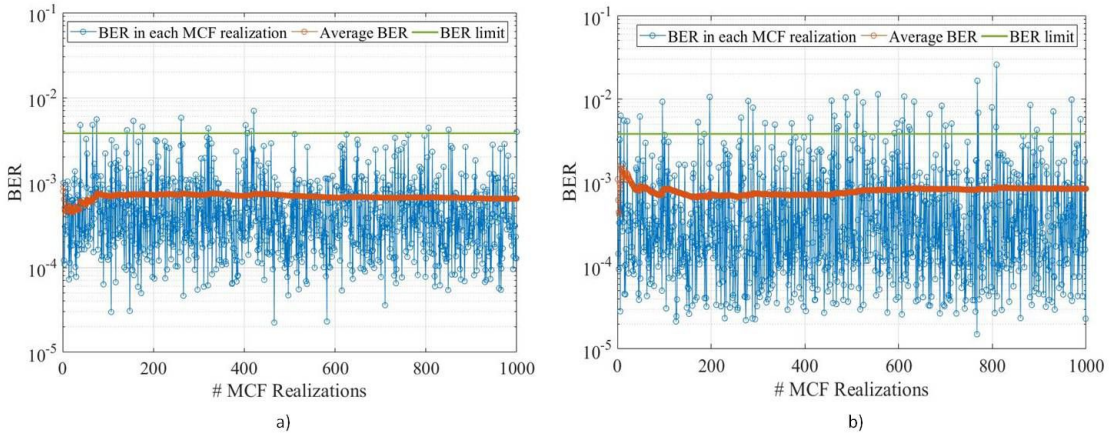

FIGURE 4.1: BER in each MCF realization and average BER as a function of the number of MCF realizations, for $r = 0$ and $X_c = -25$ dB, for a) $S_{mn}{\cdot}R_s$=1000 and b) $S_{mn}{\cdot}R_s$=0.01. The BER limit of $3.8{\times}10^{-3}$ is also depicted.

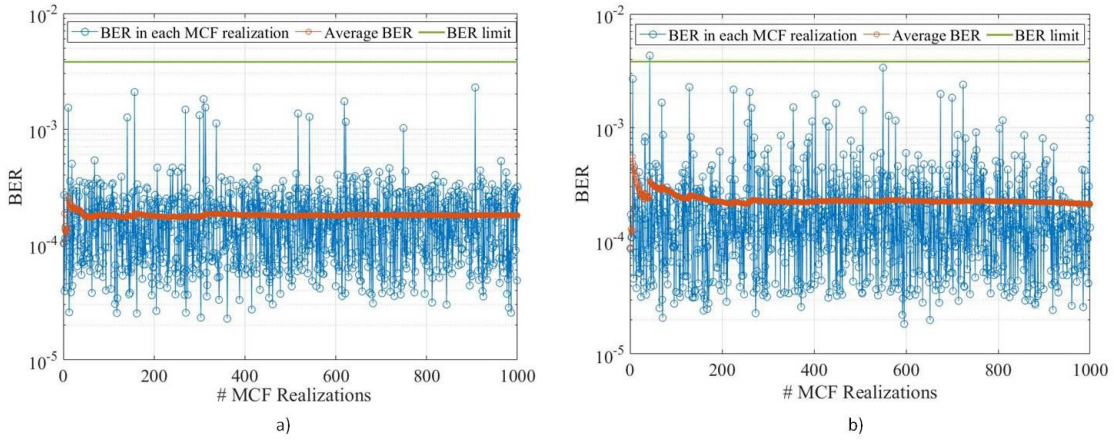

FIGURE 4.2: BER in each MCF realization and average BER as a function of the number of MCF realizations, for $r = 0$ and $X_c = -30$ dB, for a) $S_{mn}{\cdot}R_s$=1000 and b) $S_{mn}{\cdot}R_s$=0.01. The BER limit of $3.8{\times}10^{-3}$ is also depicted.

Figs. 4.1 and 4.2 show the BERs obtained in each MCF realization and the average BER as a function of the MCF realizations, for $r = 0$ and $X_c = -25$ dB and $X_c = -30$ dB, respectively, for a) $S_{mn}{\cdot}R_s$=1000 and b) $S_{mn}{\cdot}R_s$=0.01. The average BER is computed in each MCF realization by averaging the BERs per

realization calculated in previous MCF realizations. In Figs. 4.1 a) and b), the average BER is stabilized at 6.5×10^{-4} and 8.4×10^{-4}, respectively, after 1000 MCF realizations. In Fig. 4.2 a) and b), stabilized BERs of 1.8×10^{-4} and 2.3×10^{-4}, respectively, are achieved after 1000 MCF realizations. This number of MCF realizations is a conservative choice to achieve stabilized values of the average BER, as already concluded in [38], [43]. Comparatively to the work [43], where OOK optical systems have been studied, a much lower crosstalk level in PAM4 systems degrades much more the average BER in presence of ICXT than in OOK systems. In [43], for a crosstalk level of $X_c = -15$ dB and for $S_{mn}\cdot R_b$=10 and $S_{mn}\cdot R_b$=0.2, after 1000 MCF realizations, the average BER is stabilized near 10^{-3}. Figs. 4.1 and 4.2 show that in a PAM4 system, this average BER is almost reached with a crosstalk level about 10 dB lower than the one predicted for the same average BER in an OOK system. Thus, the PAM4 system performance is much more sensitive to ICXT than the OOK system performance. Regarding the OP, according to Figs. 4.1 and 4.2, we conclude that, with $X_c = -25$ dB, there are more MCF realizations that surpass the BER limit than with $X_c = -30$ dB. It is also verified that, with $S_{mn}\cdot R_s$=0.01, in 1000 MCF realizations, the BER limit is overcomed more times when compared with $S_{mn}\cdot R_s$=1000. In Fig. 4.1 a), the BER limit is exceeded about 15 times, i.e, there are 15 occurrences of the BER that lead to system outage. The OP, in this case, is approximately 0.015. With low $S_{mn}\cdot R_s$, in Fig. 4.1 b), the BER limit is exceeded about 48 times, which indicates an approximated OP of 0.048. In Fig. 4.2 a), the BER limit is never exceeded and, so, there is no outage. In 4.2 b), there are more MCF realizations with a BER closer to the BER limit, however, the BER limit is exceeded only 1 time, which results in an OP of approximately 0.001.

Through the eye-pattern analysis, it is also possible to take some conclusions regarding the impact of the ICXT on the transmission of PAM4 signals. Fig. 4.3 shows the eye-patterns at the decision circuit input for $S_{mn}\cdot R_s$=1000, $r = 0$ and $X_c = -25$ dB, for a) the worst BER (7×10^{-3}) in each MCF realization and b) the best BER (2.2×10^{-5}) in each MCF realization obtained in Fig. 4.1 a). Fig. 4.4 show the eye-patterns for $S_{mn}\cdot R_s$=0.01, $r = 0$ and $X_c = -25$ dB, for a) the worst

BER (2.5×10^{-2}) in each MCF realization and b) the best BER (1.5×10^{-5}) in each MCF realization obtained in Fig. 4.1 b). Table 4.3 shows the normalized decision thresholds F_{n1}, F_{n1} and F_{n3} and the normalized eye openings e_1, e_2 and e_3 obtained from Figs. 4.3 a) and b), 4.4 a) and b). From Figs. 4.3 and 4.4, it can be observed that, the eye-pattern in Fig. 4.4 a) shows a greater degradation due to ICXT when compared with the eye-pattern in Fig. 4.3 a), especially in the superior eye concerning the symbols '2' and '3', since the eye opening is much lower, as shown in Table 4.3. Figs. 4.3 and 4.4 b) presents much similar eye openings which are much larger than the eye openings shown in Figs. 4.3 a) and 4.4 a) due to the lower influence of ICXT for the MCF realization that leads to the best BER. Compared with Fig. 3.8 b), where the only impairment is signal distortion due mainly to fiber dispersion, the eye-patterns of Figs. 4.3 b) and 4.4 b) present very similar eye openings. Furthermore, Fig. 4.4 b) exhibits much more "well-defined" amplitude levels due to ICXT than in the eye-pattern than in Fig. 4.3 b), especially in the part of the eye where more symbol transitions occur. This effect happens because for low $S_{mn}\cdot R_s$ (Fig. 4.4 b)), only one symbol in the interfering core is contributing to ICXT, while for high $S_{mn}\cdot R_s$ (Fig. 4.3 b)), several symbols in the interfering core are contributing to ICXT. This effect has been already observed for OOK systems [38], [43]. Regarding the decision thresholds, Table 4.3 indicates that the ICXT impact does not change significantly the values of the normalized decision thresholds.

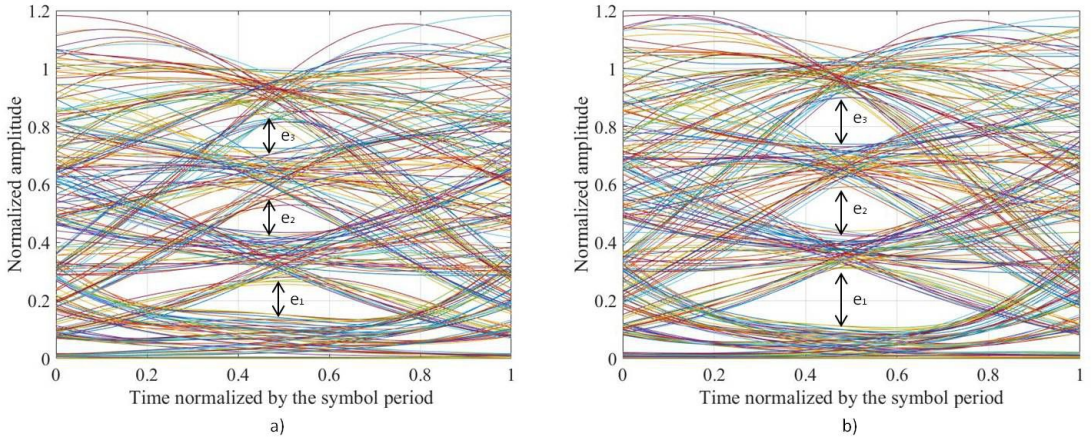

FIGURE 4.3: Eye-patterns at the decision circuit input for $S_{mn}\cdot R_s$=1000, $r = 0$ and $X_c = -25$ dB, for a) worst BER (7×10^{-3}) and b) best BER (2.2×10^{-5}) obtained in each MCF realization in Fig. 4.1 a).

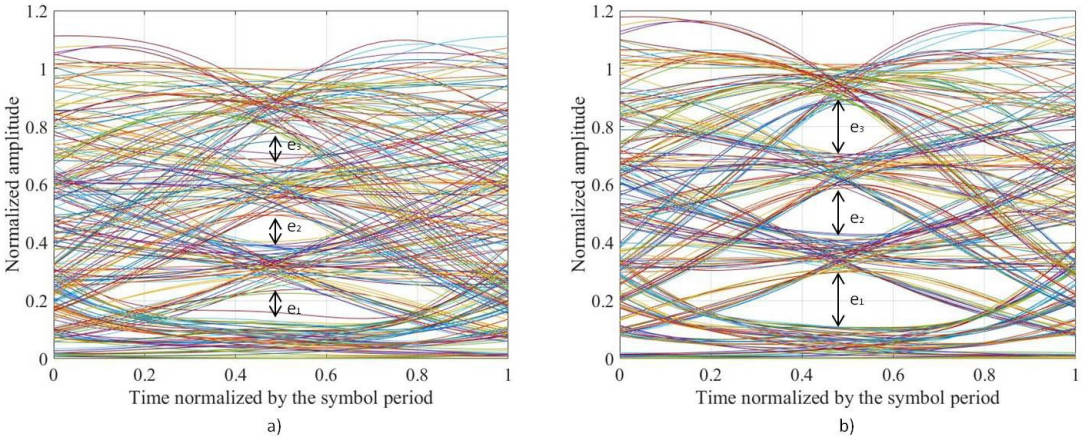

FIGURE 4.4: Eye-patterns at the decision circuit input for $S_{mn}{\cdot}R_s$=0.01, $r = 0$ and $X_c = -25$ dB, for a) worst BER ($2.5{\times}10^{-2}$) and b) best BER ($1.5{\times}10^{-5}$) obtained in each MCF realization in Fig. 4.1 b).

TABLE 4.3: Normalized decision thresholds F_{n1}, F_{n2} and F_{n3} and normalized eye openings e_1, e_2 and e_3 taken from the eye-patterns represented in Figs. 4.3 a), 4.3 b), 4.4 a) and 4.4 b).

Fig.	F_{n1}	F_{n2}	F_{n3}	e_1	e_2	e_3
4.3 a)	0.20	0.47	0.75	0.11	0.095	0.085
4.3 b)	0.21	0.52	0.82	0.20	0.15	0.16
4.4 a)	0.17	0.44	0.73	0.075	0.091	0.043
4.4 b)	0.20	0.51	0.79	0.19	0.15	0.17

Figs. 4.5 and 4.6 show the BER in each MCF realization and the average BER as a function of the number of MCF realizations, for $r = 0.1$ and the crosstalk levels of $X_c = -25$ dB and $X_c = -30$ dB, respectively, for a) $S_{mn}{\cdot}R_s$=1000 and b) $S_{mn}{\cdot}R_s$=0.01. In Figs. 4.5 a) and b), average BERs of $7.5{\times}10^{-4}$ and $3.6{\times}10^{-4}$ are achieved after 1000 MCF realizations, respectively. In Figs. 4.6 a) and b), the BER stabilizes at $1.6{\times}10^{-4}$ and $2.1{\times}10^{-4}$, respectively, after 1000 MCF realizations. For $X_c = -25$ dB, in Fig. 4.5 a), the BER limit is exceeded 2 times, which leads to an OP of about 0.002. In Fig. 4.5 b), the BER limit is exceeded 8 times which gives an OP of about 0.008. For $X_c = -30$ dB, Fig. 4.6 shows that the BERs in each MCF realization are more distant from the BER limit than in Fig. 4.2. This indicates that, for $r = 0.1$, the effect of ICXT on the OP is less detrimental than for $r = 0$. This influence of the extinction ratio on the ICXT impact on the performance has been already observed in OOK systems

[45]. The same conclusion regarding the extinction ratio influence can be taken by comparing Fig. 4.5 a) with Fig. 4.1 a), for $S_{mn}{\cdot}R_s$=1000. For $S_{mn}{\cdot}R_s$=0.01, the comparison of Fig. 4.5 b) with Fig. 4.1 b) indicates that the OP, in this case, will be higher for $r = 0.1$, about 0.008, than $r = 0$.

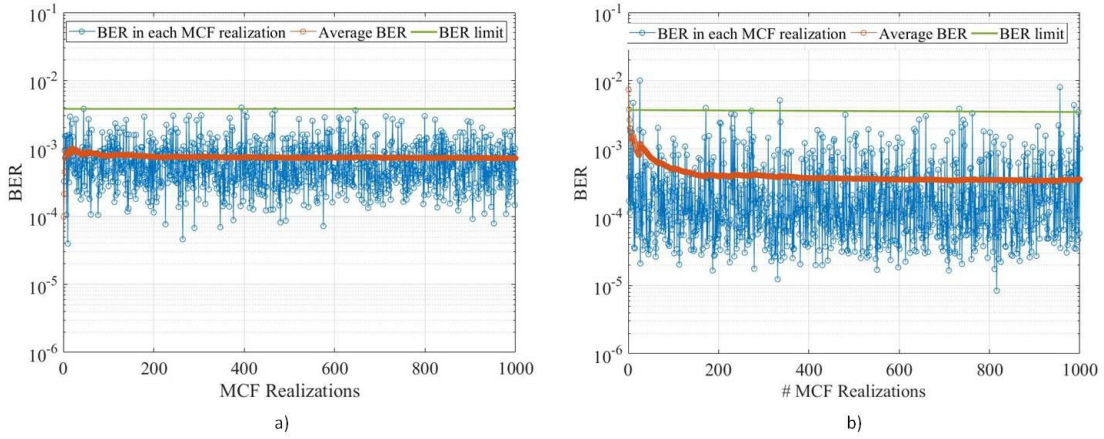

FIGURE 4.5: BER in each MCF realization and average BER as a function of the number of MCF realizations, for $r = 0.1$ and $X_c = -25$ dB, for a) $S_{mn}{\cdot}R_s$=1000 and b) $S_{mn}{\cdot}R_s$=0.01. The BER limit of $3.8{\times}10^{-3}$ is also depicted.

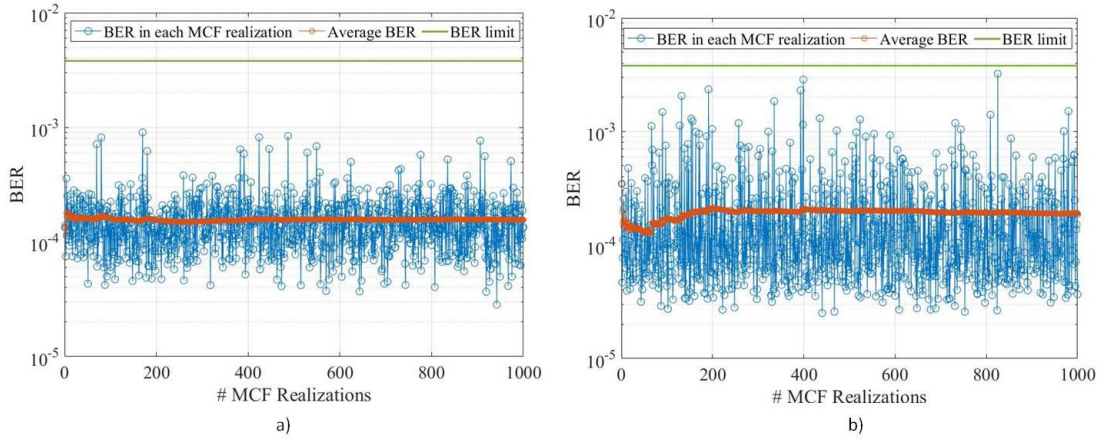

FIGURE 4.6: BER in each MCF realization and average BER as a function of the number of MCF realizations, for $r = 0.1$ and $X_c = -30$ dB, for a) $S_{mn}{\cdot}R_s$=1000 and b) $S_{mn}{\cdot}R_s$=0.01. The BER limit of $3.8{\times}10^{-3}$ is also depicted.

Fig. 4.7 shows the eye-patterns obtained for $S_{mn}{\cdot}R_s$=1000, $r = 0.1$ and $X_c = -25$ dB, for a) the worst BER ($4{\times}10^{-3}$) in each MCF realization and for b) the best BER ($4{\times}10^{-5}$) in each MCF realization in Fig. 4.5 a). Fig. 4.8 shows the eye-patterns at the decision input circuit, obtained for $S_{mn}{\cdot}R_s$=0.01, $r = 0.1$ and $X_c = -25$ dB, for a) the worst BER ($1{\times}10^{-2}$) in each MCF realization and for b) the best BER ($8.4{\times}10^{-6}$) in each MCF realization in Fig. 4.5 b). Table 4.4 shows the normalized decision thresholds F_{n1}, F_{n1} and F_{n3} and the normalized

eye openings e_1, e_2 and e_3 obtained for Figs. 4.7 a), 4.7 b), 4.8 a) and 4.8 b). In Figs. 4.7 a) and 4.8 a), it can be observed that, with $S_{mn}{\cdot}R_s$=0.01, there is a very high degradation of the eye-pattern due to the ICXT impairment than with $S_{mn}{\cdot}R_s$=1000, as the superior eye regarding symbols '2' and '3' in Fig. 4.8 a) is completely closed due to the ICXT influence. The eye-pattern in Fig. 4.7 a) presents a much similar eye opening when compared with Fig. 4.8 a), and both eye openings are much larger than the eye openings presented in Figs. 4.7 b) and 4.8 b) due to the residual impact of ICXT. The eye openings are very similar to the eye openings presented in Fig. 3.8 b), where the only impairment is the signal distortion due to fiber dispersion. Again, the decision thresholds are not much affected by the impact of ICXT.

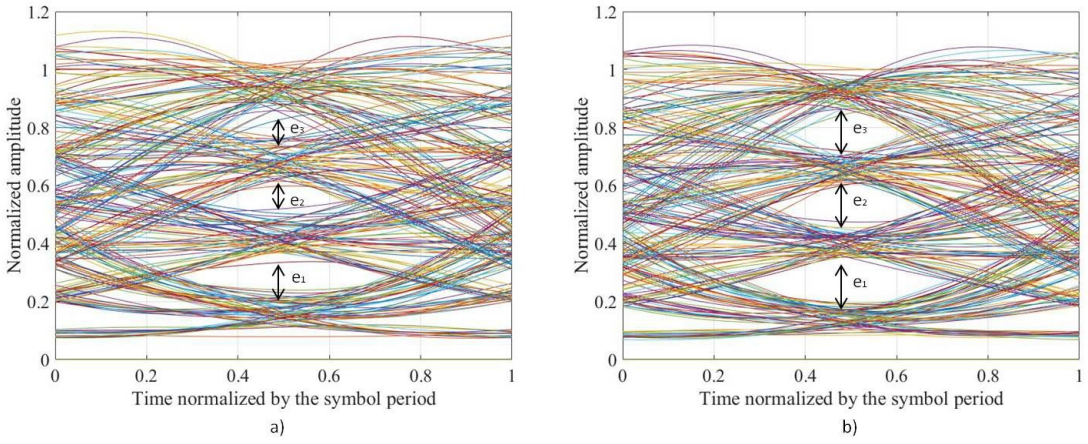

FIGURE 4.7: Eye-patterns at the decision circuit input corresponding to $S_{mn}{\cdot}R_s$=1000, for $r = 0.1$ and $X_c = -25$ dB for a) worst BER ($4{\times}10^{-3}$) and b) best BER ($4{\times}10^{-5}$) obtained in each MCF realization in Fig. 4.5 a).

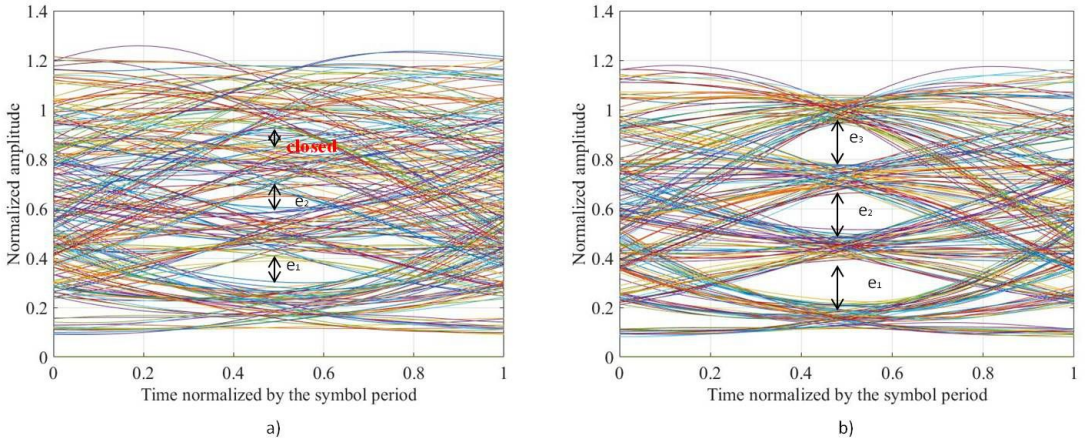

FIGURE 4.8: Eye-patterns at the decision circuit input corresponding to $S_{mn}{\cdot}R_s$=0.01, for $r = 0.1$ and $X_c = -25$ dB for a) worst BER ($1{\times}10^{-2}$) and b) best BER ($8.4{\times}10^{-6}$) obtained in each MCF realization in Fig. 4.5 b).

TABLE 4.4: Normalized decision thresholds F_{n1}, F_{n2} and F_{n3} and normalized eye openings e_1, e_2 and e_3 for Figs. 4.7 a), 4.7 b), 4.8 a) and 4.8 b).

Fig.	F_{n1}	F_{n2}	F_{n3}	e_1	e_2	e_3
4.7 a)	0.29	0.55	0.80	0.098	0.079	0.067
4.7 b)	0.27	0.53	0.78	0.16	0.13	0.13
4.8 a)	0.34	0.62	closed	0.086	0.0459	closed
4.8 b)	0.31	0.58	0.846	0.17	0.15	0.16

4.4 Power penalty due to ICXT

In this section, the degradation of the average BER caused by ICXT in a PAM4 short-haul link is studied. As such, the number of MCF realizations required for the average BER to stabilize considered in the following studies is 1000. The target average BER without crosstalk of 3.8×10^{-3} is achieved with an optical power at the optical fiber input of -25.7 dBm, for $r = 0$, and -24.8 dBm, for $r = 0.1$, respectively.

The performance metric used to study the degradation caused by ICXT on the average BER is the power penalty [38], [43]. The power penalty, in dB, corresponds, to the difference of the signal power required to obtain a target BER in presence of ICXT, for a specific ICXT level, and the signal power required to reach the same BER in absence of ICXT. In this work, we consider a threshold power penalty of 1 dB [38], [43]. In each simulation, for each ICXT level, the optical signal power at the optical fiber input is increased until the target average BER is reached. Then, this optical signal power obtained for a specific ICXT level is subtracted by the optical signal power required to reach the target average BER in absence of ICXT. Fig. 4.9 exemplifies this procedure. Fig. 4.9 shows the average BER as a function of the crosstalk level for $S_{mn}\cdot R_s$=1000 and $S_{mn}\cdot R_s$=0.01, $r = 0.1$, and is obtained for an optical power at the optical fiber input of -24.2 dBm and -23.6 dBm, respectively, which are the required optical powers to reach the target average BER in presence of ICXT with a crosstalk level

of $X_c = -26$ dB. The power penalties obtained, in this example, are 0.6 dB and 1.2 dB for $r = 0.1$ and $S_{mn}{\cdot}R_s$=1000 and $S_{mn}{\cdot}R_s$=0.01, respectively.

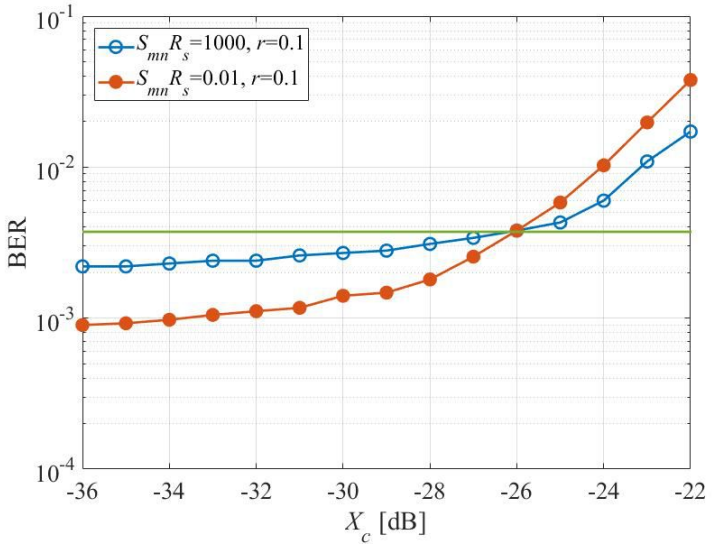

FIGURE 4.9: Average BER as a function of crosstalk level X_c, for $S_{mn}{\cdot}R_s$=1000 and $r = 0.1$. The BER limit of $3.8{\times}10^{-3}$ is also shown (green line).

Fig. 4.10 shows the power penalty as a function of the ICXT level obtained for $S_{mn}{\cdot}R_s$=1000 and $S_{mn}{\cdot}R_s$=0.01, and $r = 0$ and $r = 0.1$. Fig. 4.10 shows that the power penalty degradation due to ICXT is more enhanced for $S_{mn}{\cdot}R_s$=0.01 than for $S_{mn}{\cdot}R_s$=1000, as already observed in OOK systems [38], [43]. For $r = 0.1$ (and $S_{mn}{\cdot}R_s$=0.01), this degradation reaches almost 3 dB for a ICXT level of -25 dB. Considering the power penalty of 1 dB as the limit, this power penalty is reached with a crosstalk level of about $X_c = -23$ dB for $S_{mn}{\cdot}R_s$=1000 and $r = 0$, $X_c = -25.3$ dB, for $S_{mn}{\cdot}R_s$=0.01 and $r = 0$, $X_c = -23.7$ dB for $S_{mn}{\cdot}R_s$=1000 and $r = 0.1$ and $X_c = -26.4$ dB for $S_{mn}{\cdot}R_s$=0.01 and $r = 0.1$. For $r = 0.1$ a lower ICXT level is required to achieve the 1 dB of power penalty than for $r = 0$, regardless of the $S_{mn}{\cdot}R_s$ considered. There is a difference between the crosstalk levels obtained with the two extinction ratios of 0.7 dB for $S_{mn}{\cdot}R_s$=1000 and 1.1 db for $S_{mn}{\cdot}R_s$=0.01. Fig. 4.10 shows that the crosstalk levels that lead to a power penalty degradation of 1 dB with low $S_{mn}{\cdot}R_s$ are at least 2.3 dB above the ones found with high $S_{mn}{\cdot}R_s$. In OOK optical systems [38], [43], the power penalty of 1 dB has been achieved with much higher crosstalk levels, $X_c = -14.3$ dB and $X_c = -12.9$ dB for $S_{mn}{\cdot}R_s$=10 and $S_{mn}{\cdot}R_b$=0.02, respectively, with $r = 0$.

Thus, in PAM4 systems, the ICXT levels that lead to a power penalty of 1 dB are more than 9 dB below the ones found for an OOK system. This leads to the conclusion that PAM4 systems with direct-detection are much more susceptible to the degradation induced by ICXT than OOK systems with direct-detection.

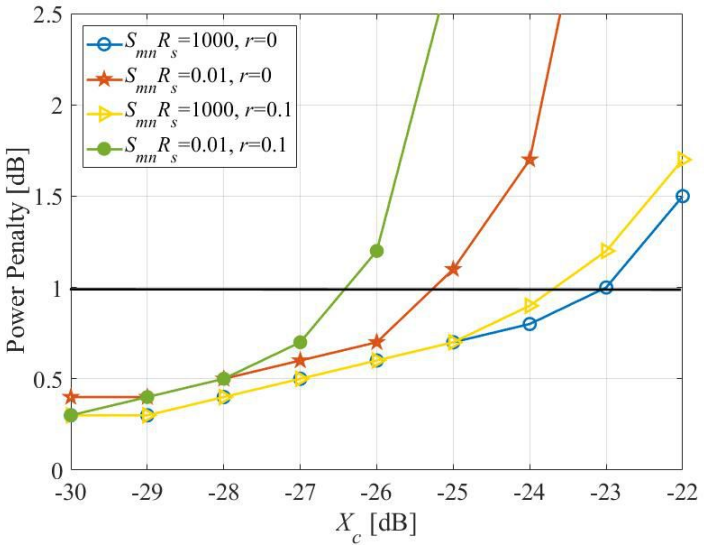

FIGURE 4.10: Power penalty as a function of crosstalk level X_c, for $r = 0.1$ and $S_{mn}{\cdot}R_s$=1000 and $S_{mn}{\cdot}R_s$=0.01. The threshold power penalty of 1 dB is also shown (black line).

4.5 Outage probability

The outage probability is the probability of a system becoming unavailable when a target BER limit is reached [45], [46]. In this work, the system is considered unavailable, i.e, is in an outage period, when the BER in presence of ICXT surpasses the BER limit of $3.8{\times}10^{-3}$. In the simulation, the OP is estimated by [38]

$$OP = \frac{N_o}{N_r} \tag{4.1}$$

where N_o is the number of occurrences of BER above the BER limit and N_r is the number of simulated MCF realizations necessary to reach this number of occurrences. An acceptable outage probability in optical communications is typically lower than 10^{-4} [46], [47].

4.5.1 Dependence of the OP on the number of MCF realizations

In this subsection, we verify the OP dependence on the number of MCF realizations, for several $S_{mn}{\cdot}R_s$, extinction ratios and crosstalk levels.

Fig. 4.11 shows the OP as a function of the number of MCF realizations, for $r = 0$, and a) $S_{mn}{\cdot}R_s$=1000 and $X_c = -26$ dB; b) $S_{mn}{\cdot}R_s$=0.01 and $X_c = -26$ dB and c) $S_{mn}{\cdot}R_s$=0.01 and X_c=-28.2 dB. Notice that Fig. 4.11 a) and b) have the same parameters that lead to a power penalty of 1 dB as shown in Fig. 4.9. The BER is estimated in each MCF realization and the simulation is stopped when the number of occurrences of BER above the BER limit reaches 200, where we consider that the OP has been estimated with sufficient accuracy [38], [45]. In Figs. 4.11 a) and c), the oscillations of the OP estimates extend over a higher number of MCF realizations than in Fig. 4.11 b). According to Figs. 4.11 a) and b), it is possible to observe that for the same crosstalk level and extinction ratio, a higher number of MCF realizations is needed to reach 200 occurrences of BER above the BER limit, with $S_{mn}{\cdot}R_s$=1000 than with $S_{mn}{\cdot}R_s$=0.01, since the OP of the system with the higher $S_{mn}{\cdot}R_s$, about $4{\times}10^{-3}$, is one order of magnitude lower than the one shown in Fig. 4.11 b) of about $2{\times}10^{-2}$. In Fig. 4.11 c), with $S_{mn}{\cdot}R_s$=0.01 and $X_c = -28.2$ dB, it is possible to observe that the number of MCF realizations is nearly the same as in Fig. 4.11 a), since the values of OP reached after 200 occurrences in both figures are very similar. Fig. 4.11 indicates that the number of MCF realizations necessary to estimate the OP with sufficient accuracy only depends on the order of magnitude of the OP as already hinted in other works [38], [43], [45]. In [43], the number of occurrences for which it is possible to obtain an outage probability of the optical communication system with very small fluctuations has been assessed for an OOK system, and it has been concluded that 200 occurrences are more than enough to achieve this goal. Thus, in this work, in all studies involving the OP estimation, N_o=200 are considered, which as shown in Fig. 4.11 are more than enough to obtain a stabilized value of the OP for PAM4 systems with direct-detection.

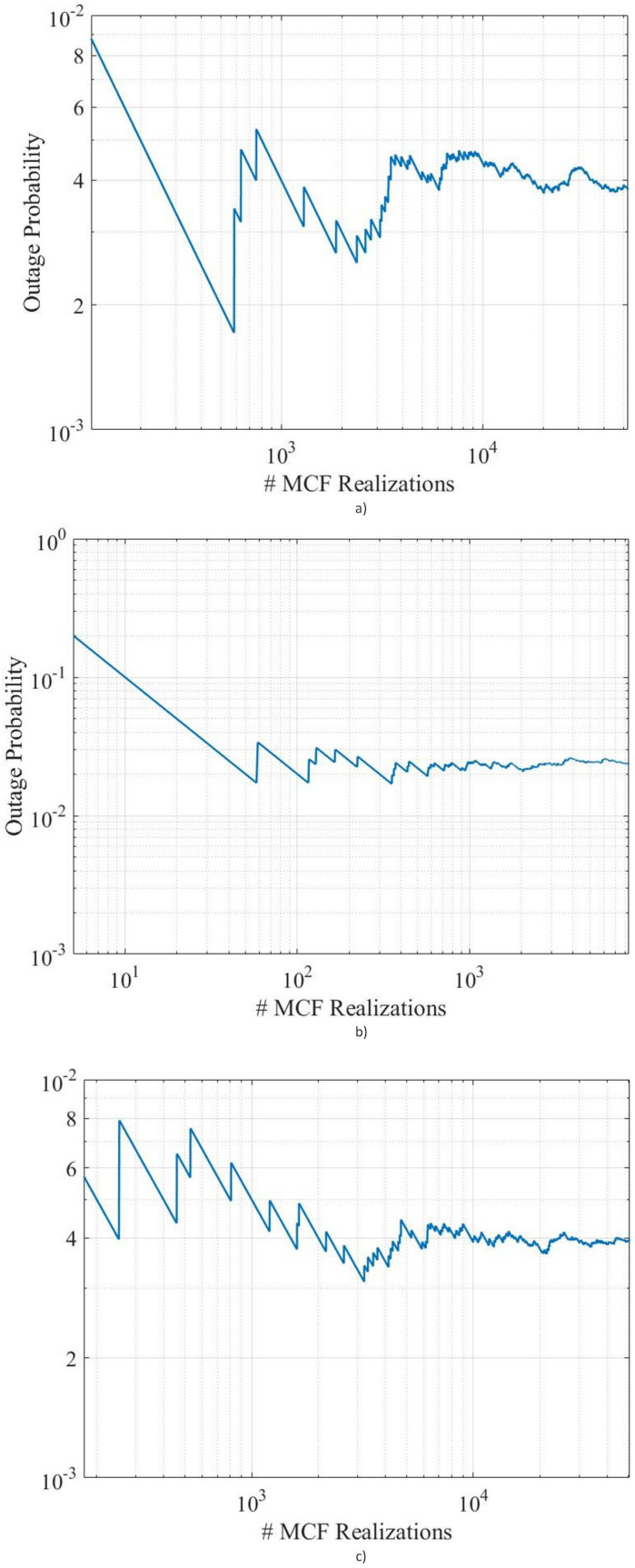

FIGURE 4.11: Outage probability as a function of the number of MCF realizations, for $r = 0$ and a) $S_{mn} \cdot R_s$=1000 and $X_c = -26$ dB; b) $S_{mn} \cdot R_s$=0.01 and $X_c = -26$ dB and c) $S_{mn} \cdot R_s$=0.01 and $X_c = -28.2$ dB.

4.5.2 OP for λ=1550 nm and one interfering core

In this subsection, we assess the OP in PAM4 systems with direct-detection, for a single interfering core, λ=1550 nm, for low and high $S_{mn}{\cdot}R_s$ and $r = 0$ and $r = 0.1$. A comparison with the power penalties due to ICXT of 1 dB obtained in subsection 4.4 is also established.

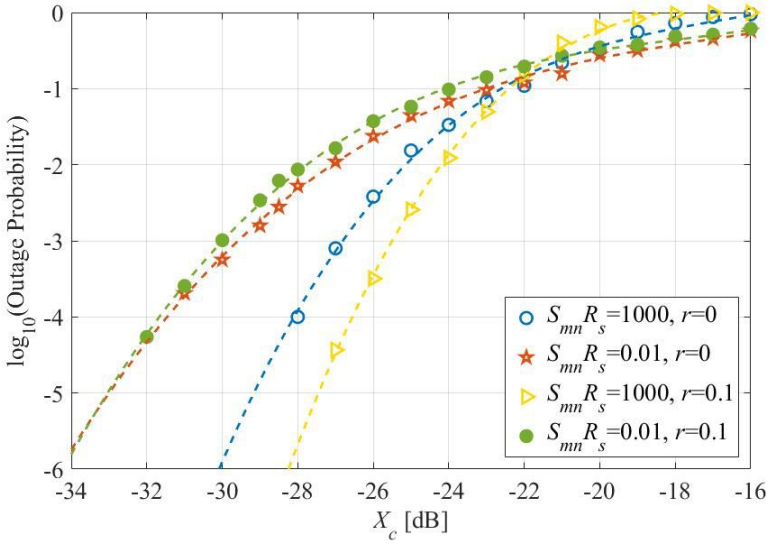

FIGURE 4.12: Outage probability as a function of X_c, for $S_{mn}{\cdot}R_s$=1000 and $r = 0$; $S_{mn}{\cdot}R_s$=0.01 and $r = 0$; $S_{mn}{\cdot}R_s$=1000 and $r = 0.1$ and $S_{mn}{\cdot}R_s$=0.01 and $r = 0.1$. The dashed lines represent a cubic interpolation of the $\log_{10}(\ )$ of the outage probability.

Fig. 4.12 shows the OP as a function of the ICXT level, for λ =1550 nm, D_λ =17 ps/(nm·km), L = 2 km, $S_{mn}{\cdot}R_s$=1000 and $r = 0$; $S_{mn}{\cdot}R_s$=0.01 and $r = 0$; $S_{mn}{\cdot}R_s$=1000 and $r = 0.1$ and $S_{mn}{\cdot}R_s$=0.01 and $r = 0.1$ obtained by simulation. For $X_c \geq -22$ dB, the system is unavailable with a very high OP above 10^{-1}. Hence, for PAM4 systems impaired by ICXT due to one interfering core, ICXT levels above this value are prohibitive. For lower crosstalk levels, with $S_{mn}{\cdot}R_s$=1000, for a BER limit of 10^{-3}, for example, a higher crosstalk level is needed to achieve this OP than with $S_{mn}{\cdot}R_s$=0.01, regardless of the extinction ratio. So, for high $S_{mn}{\cdot}R_s$, Fig 4.12 indicates that the system is more robust to outage than for lower $S_{mn}{\cdot}R_s$, as already concluded in [38], [43], [45] for OOK signalling. For $S_{mn}{\cdot}R_s$=0.01, comparing $r = 0$ with $r = 0.1$, the higher extinction ratio presents slightly higher OPs for the same crosstalk level. This suggests that, for $S_{mn}{\cdot}R_s \ll 1$, the influence of the extinction ratio on the OP is not much relevant.

By comparating with OOK systems [38], [43], a much higher ICXT level is needed to achieve the same outage probability in the PAM4 direct-detection system. For example, the crosstalk levels of $X_c = -18$ dB and $X_c = -22$ dB [38], [43], lead to an outage probability of 10^{-3}, in OOK optical systems, with $r = 0$ and $S_{mn}{\cdot}R_b$=10 and $S_{mn}{\cdot}R_b$=0.02, respectively. As can be seen in Fig. 4.12, in PAM4 systems, the ICXT level that leads to this outage probability is much lower, $X_c = -26.9$ dB, for the higher $S_{mn}{\cdot}R_s$, which is 8.9 dB lower than in OOK systems, and $X_c = -29.6$ dB for the lower $S_{mn}{\cdot}R_s$, which is 7.6 dB lower than in OOK systems. Since the simulation takes a long time to reach lower outage probabilities, around 10^{-4}, the OP obtained for $X_c = -28$ dB, $S_{mn}{\cdot}R_s$=1000 and $r = 0$, has been obtained with only 100 occurrences and, for $X_c = -27$ dB, $S_{mn}{\cdot}R_s$=1000 and $r = 0.1$, the OP has been obtained with 47 occurrences. In this case, these simulations took more than one week to achieve 100 and 47 occurrences, respectively. As very low OPs ($\ll 10^{-4}$) are computationally heavy to achieve using computer simulation, we have performed a cubic interpolation of the $\log_{10}$(OP), to achieve such lows OPs, similarly to what has been done in [38].

TABLE 4.5: Maximum crosstalk level to achieve 1 dB power penalty or an outage probability of 10^{-4}, for $r = 0$.

Performance metric	$S_{mn}{\cdot}R_s$=1000	$S_{mn}{\cdot}R_s$=0.01
Power penalty of 1 dB	−23 dB	−25.3 dB
Outage probability of 10^{-4}	−28 dB	−31.5 dB

TABLE 4.6: Maximum crosstalk level to achieve 1 dB power penalty or an outage probability of 10^{-4}, for $r = 0.1$.

Performance metric	$S_{mn}{\cdot}R_s$=1000	$S_{mn}{\cdot}R_s$=0.01
Power penalty of 1dB	−23.7 dB	−26.4 dB
Outage probability of 10^{-4}	−26.6 dB	−31.7 dB

Tables 4.5 and 4.6 shows the required ICXT level, to achieve a power penalty of 1 dB or an OP of 10^{-4}, for high and low $S_{mn}{\cdot}R_s$, $r = 0$ and $r = 0.1$, respectively. Tables 4.5 and 4.6 show that the power penalty can be a very poor metric to assess the impact of ICXT on the system, since for the crosstalk levels that lead to a 1 dB power penalty (above −26.5 dB), the PAM4 system is probably unavailable

with an OP above 10^{-2}. As already concluded for OOK systems, it is essential to study the OP for direct-detection optical systems impaired by ICXT, since even if the average BER is set within prescribed limits, the system can be unavailable with very high probability.

4.5.3 OP dependence on the chromatic dispersion

In intra-datacenter links, as the reach is very short (below 10 km), the optical communication system typically operates near the 1310 nm wavelength to minimize total chromatic dispersion [3]. All studies performed previously in this work have considered that the PAM4 system was working at λ =1550 nm, where the optical attenuation is minimized. In this subsection, the OP is studied for a different fiber transmission window, λ =1310 nm, assuming near zero dispersion, D_λ =1 ps/(nm·km) and a fiber length of L =2 km.

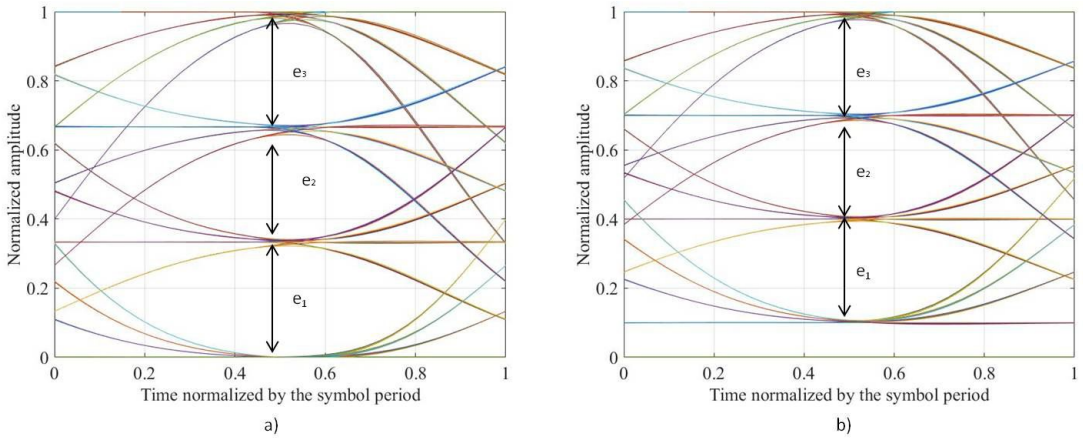

FIGURE 4.13: Eye-patterns at the decision input for λ=1310 nm and L= 2 km and a) $r = 0$ and b) $r = 0.1$.

Figs. 4.13 a) and b) present the eye-patterns at the decision circuit input for L= 2 km and $r = 0$ and $r = 0.1$, respectively. Comparing to Fig. 3.8 b) and Fig. 3.9 b), it can be concluded that, in Figs. 4.13 a) and b), the impact of chromatic dispersion is practically negligible and the eye-patterns are very similar to the ones obtained for L= 0 km (see Figs. 3.8) a) and 3.9 a)). In Fig. 4.13 a), the normalized decisions thresholds F_{n1}, F_{n2}, F_{n3} are 0.1660, 0.4961 and 0.8221, respectively, and the normalized eye openings e_1=0.3208, e_2=0.3027 and e_3=0.2943. In Fig. 4.13 b),

the normalized decisions thresholds are F_{n1}=0.2522, F_{n2}=0.5483 and F_{n3}=0.8426 and the normalized eye openings are e_1, e_2, e_3 are 0.2867, 0.2778 and 0.2724, respectively.

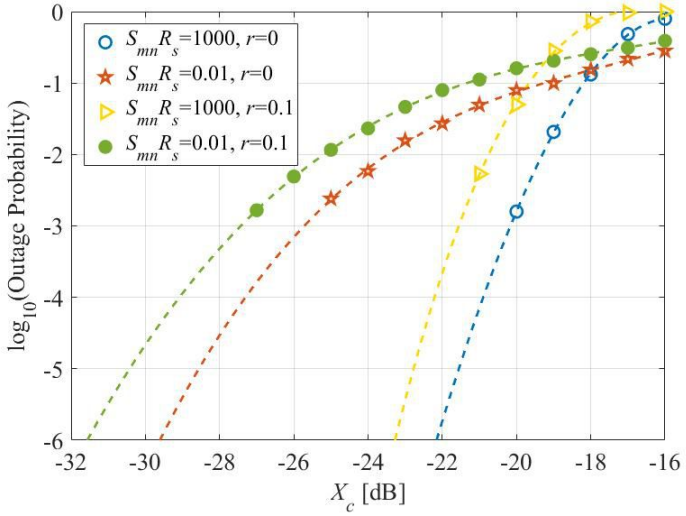

FIGURE 4.14: Outage probability as a function of X_c, for $r = 0$ and $r = 0.1$, $S_{mn}{\cdot}R_s$=1000 and $S_{mn}{\cdot}R_s$=0.01, for λ=1310 nm. The dashed lines represent a cubic interpolation of the $\log_{10}(\ )$ of the outage probability.

Fig. 4.14 shows the OP as a function of the ICXT level for λ =1310 nm, $S_{mn}{\cdot}R_s$=1000 and $r = 0$; $S_{mn}{\cdot}R_s$=0.01 and $r = 0$; $S_{mn}{\cdot}R_s$=1000 and $r = 0.1$ and $S_{mn}{\cdot}R_s$=0.01 and $r = 0.1$ obtained by simulation. Fig. 4.12, obtained for λ=1550 nm, and Fig. 4.14 indicate that in presence of ICXT, the interaction of chromatic dispersion with ICXT affect significantly the OP. Comparing to Fig. 4.12, the system requires a much higher ICXT level to achieve the same OP. For example, to achieve an OP 10^{-4}, for $r = 0$, the system needs an ICXT level of -20.9 dB and -27.3 dB for $S_{mn}{\cdot}R_s$=1000 and $S_{mn}{\cdot}R_s$=0.01, respectively, which is 7.1 dB and 4.2 dB higher than in Fig. 4.12. For $r = 0.1$, ICXT levels of -22.2 dB and -29.1 dB are required, respectively, to reach the reference OP of 10^{-4}, for $S_{mn}{\cdot}R_s$=1000 and $S_{mn}{\cdot}R_s$=0.01. These ICXT levels are 4.4 dB and 2.6 dB higher than the ones shown in Fig- 4.12. So, Fig. 4.14 demonstrates, that, for λ=1310 nm, where chromatic dispersion is residual, the PAM4 system is much more tolerant to ICXT than for λ=1550 nm, with an improved tolerance of at least 2.5 dB. The severe chromatic dispersion observed for λ=1550 nm is responsible for the tolerance reduction.

4.5.4 Dependence of the OP on the number of interfering cores

All previous results regarding the OP have only considered one interfering core. In a MCF, there are several cores that contribute to ICXT [10]. In a weakly-coupled MCF, the number of interfering cores that have a significant contribution to ICXT on one specific interfered core is typically below 8 which are typically the neighbouring cores at closer distance (with lower core pitch) to the interfered core [48]. In this subsection, the OP is assessed for several interfering cores, λ =1550 nm and $S_{mn}{\cdot}R_s$=1000.

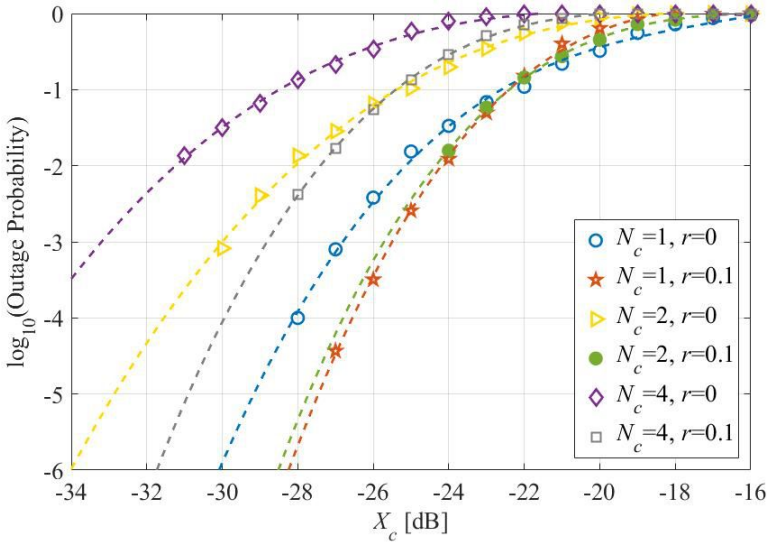

FIGURE 4.15: Outage probability as a function of X_c, for $r = 0$ and $r = 0.1$, $S_{mn}{\cdot}R_s$=1000 and N_c= 1, 2, 4.

Fig. 4.15 shows the OP as a function of the ICXT level, for $r = 0$ and 0.1, $S_{mn}{\cdot}R_s$=1000 and for N_c= 1, 2, 4 interfering cores, obtained from simulation. Fig. 4.15 shows a clear degradation of the OP with the increase of the number of interfering cores. For N_c=2, $r = 0$ and $X_c \geq -25$ dB, the system is unavailable with a very high OP above 10^{-1}. For $r = 0.1$, the same happens for $X_c \geq -22$ dB. For N_c=4, $r = 0$ and $X_c \geq -29$ dB, the system is unavailable with a very high OP above 10^{-1}. For $r = 0.1$, the same happens for X_c above near -25 dB. The crosstalk levels that leads to an OP of 10^{-3}, for N_c=1, N_c=2 and N_c=4, are, respectively, -26.9 dB, -30.4 dB, -33 dB, for $r = 0$, and -25.5 dB, -25.7 dB, -28.7 dB, for $r = 0.1$. This indicates a crosstalk level decrease of nearly 3 dB,

when doubling the interfering core count, for $r = 0$. For $r = 0.1$, there is a crosstalk level decrease of 3 dB, when passing from N_c=2 to N_c=4, but the OPs obtained with one and two interfering cores are very similar.

X_c [dB]	N_c=1, $r = 0$	N_c=1, $r = 0.1$	N_c=2, $r = 0$	N_c=2, $r = 0.1$	N_c=4, $r = 0$	N_c=4, $r = 0.1$
-20	8 min	4 min	4 min	8 min	8 min	8 min
-22	23 min	17 min	5 min	26 min	8 min	11 min
-24	1 h 16 min	3 h 27 min	17 min		10 min	26 min
-26	9 h 44 min	5 days			23 min	
-27	35 h 37 min	–			35 min	
-28	1 week	–	4 h		1 h 10 min	30 h 30min
-29	–	–	16 h		2h	–
-30	–	–	–			–
-31	–	–	–		8 h	–

TABLE 4.7: Simulation times required to obtain the OPs in Fig. 4.15 for $r = 0$, $r = 0.1$, $S_{mn}{\cdot}R_s$=1000 and N_c= 1, 2, 4, for several crosstalk levels.

Table 4.7 shows the simulation times took to reach the OPs shown in Fig. 4.15 for several crosstalk levels, for $r = 0$, $r = 0.1$, $S_{mn}{\cdot}R_s$=1000 and N_c= 1, 2, 4. From Table 4.7, it is clear that the simulation time is very dependent on the magnitude of the OP. Considering $r = 0$ and $N_c = 1$, for the crosstalk levels of -22 dB (OP=10^{-1}); -24 dB (OP=$10^{-1.5}$) and -26 dB (OP=$10^{-2.4}$), the simulation times increase, respectively, from 23 min, to 1 h and almost 10 h, respectively. For the same OP level, for example, OP=10^{-3} and $r = 0$, which correspond to crosstalk levels of -25 dB, -28 dB and -31 dB, respectively, for N_c= 1, 2 and 4, the simulation time increases by a factor near 2, when the number of interfering cores doubles.

To understand the results obtained in Fig. 4.15, with $r = 0.1$ and N_c= 1,2, in which the OPs obtained are very similar and there is a significant OP degradation with N_c=4, we have obtained the BER as a function of the number of MCFs realizations for those cores. Fig. 4.16 shows the BERs obtained in each MCF

realization and the average BER as a function of the MCF realizations, for $r = 0.1$, $X_c = -24$ dB and $S_{mn} \cdot R_s$=1000 for a) N_c= 1, b) N_c= 2 and c) N_c= 4. In Figs. 4.16 a), b) and c), the average BERs of 1×10^{-3}, 8.9×10^{-4} and 3.1×10^{-3} are achieved after 1000 realizations, respectively. According to Fig. 4.15, in Fig. 4.16 a), the BER limit is exceeded 18 times, which leads to an OP of about 0.018. In Fig. 4.16 b), the BER limit is exceeded 19 times, which gives an OP of about 0.019. In Fig. 4.16 c), the BER limit is exceeded much more times than in Figs. 4.16 a) and b), which gives a much higher OP. All these analysis are in accordance with the results presented in Fig. 4.15.

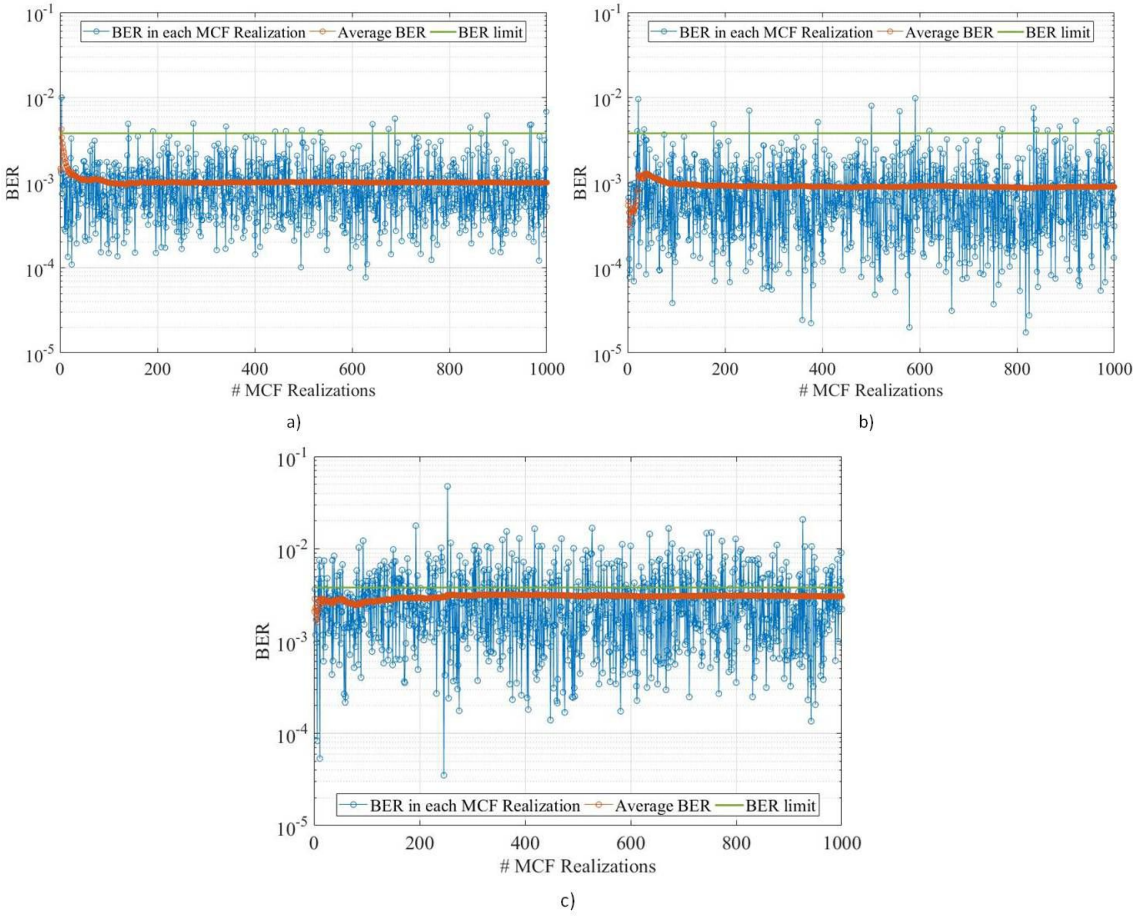

FIGURE 4.16: BER in each MCF realization and average BER as a function of the number of MCF realizations, for $r = 0.1$, $X_c = -24$ dB and $S_{mn} \cdot R_s$=1000 for a) N_c= 1, b) N_c= 2 and c) N_c= 4. The BER limit of 3.8×10^{-3} is also depicted.

4.5.5 Dependence of the OP on the time misalignment between signals

In real systems, the transitions between the symbols of the PAM4 signal at the input of the interfered and interfering cores are hardly aligned on time. The studies performed in previous sections have assumed aligned symbols at the MCF cores inputs. In this subsection, the influence of the time misalignment between symbols in different cores on the OP is assessed for a single interfering core and λ =1550 nm. The time misalignments considered are submultiples of the symbol period T_s and are characterized by $\Delta\tau{=}MT_s$, where M defines the ratio of misalignment with respect to the interfered core. For example, with $M{=}0$ or $M{=}1$, the transitions between the symbols are aligned in both cores.

Fig. 4.17 shows the OP as a function of the ICXT level, for $r = 0$ and several time misalignments, for a) $S_{mn}{\cdot}R_s{=}1000$ and b) $S_{mn}{\cdot}R_s{=}0.01$, obtained by MC simulation. Fig. 4.17 a) shows that, for high $S_{mn}{\cdot}R_s$, the OP dependence on the time misalignment is practically negligible. This result has been already found in OOK systems with direct-detection [45]. With $S_{mn}{\cdot}R_s{\gg}1$, there are several symbols of the interfering core that contribute to ICXT (for example, for $S_{mn}{\cdot}R_s{=}1000$, roughly one thousand symbols affect one symbol in the interfered core), and the relative misalignment of the symbols practically does not affect the OP. For $S_{mn}{\cdot}R_s{=}0.01$, only one symbol of the interfered core contributes to the ICXT on the interfered core. As shown in Fig. 4.17 b), in this case, the OP is much more dependent on the time misalignment. Fig. 4.17 b) shows also that a time misalignment of half the symbol period, $M{=}1/2$, leads to the lower OP. Aligned symbols, $M{=}0$ or $M{=}1$, decrease the tolerance to ICXT of the PAM4 system. These conclusions regarding the time misalignment for $S_{mn}{\cdot}R_s{\ll}1$ have been already reported in [45] for OOK systems.

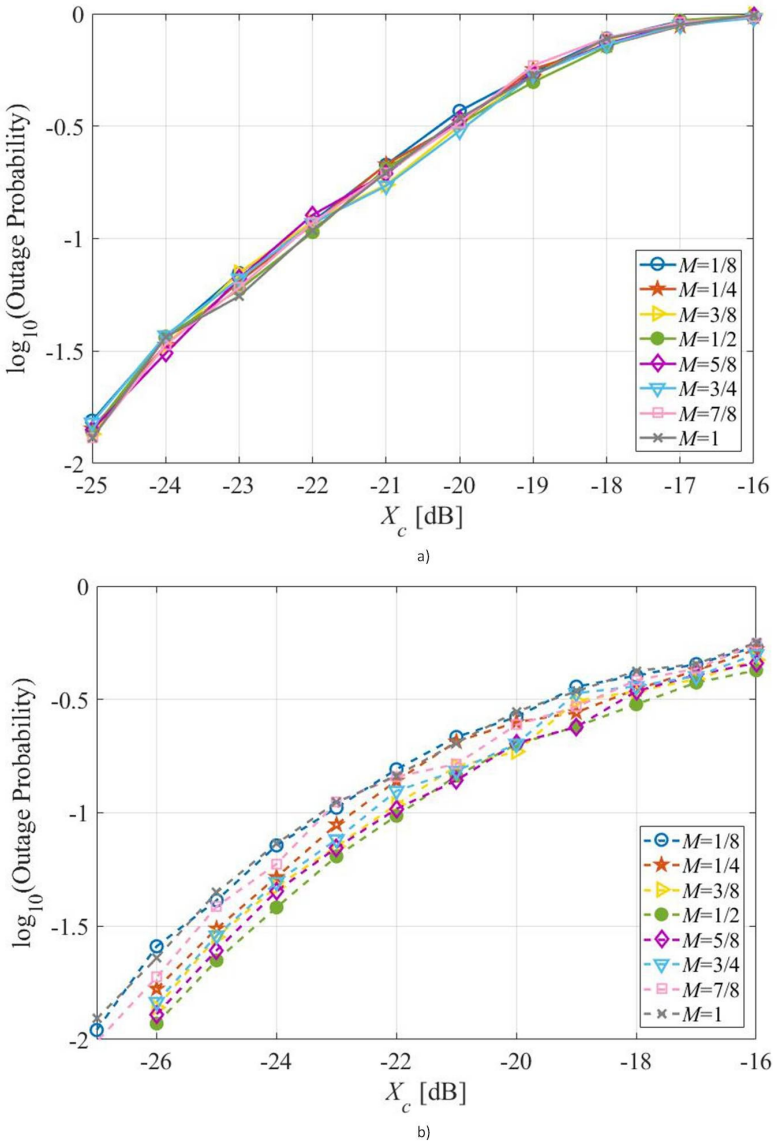

FIGURE 4.17: Outage probability as a function of the crosstalk level X_c, for $r = 0$ and M= 1/8, 1/4, 3/8, 1/2, 5/8, 3/4, 7/8 and 1, for a) $S_{mn}{\cdot}R_s$=1000 and b) $S_{mn}{\cdot}R_s$=0.01.

4.6 Conclusions

In this chapter, the impact of ICXT on the performance of PAM4 signals in short direct-detection links was studied through MC simulation. We have shown that a number of MCF realizations of 1000 is more than enough to obtain a stabilized average BER of the PAM4 system.

The impact of ICXT on the received PAM4 signals has been also studied through the eye-pattern analysis. For both high and low $S_{mn}{\cdot}R_s$, and concerning the best achievable BER in one MCF realization, the eye openings are much similar to the one obtained in B2B configuration, due to the lower influence of ICXT for the MCF realization that leads to the best BER. Regarding the worst BER, for low $S_{mn}{\cdot}R_s$, the eye-patterns exhibit much more "well-defined" amplitude levels due to ICXT. It was also concluded that the ICXT does not have much impact on the normalized decision thresholds.

The power penalty due to ICXT was also studied and, as such, a threshold power penalty of 1 dB has been considered as a reference. It was concluded that, to reach the power penalty of 1 dB, for $r = 0$, ICXT levels of -23 dB and -25.3 dB, are necessary for $S_{mn}{\cdot}R_s$=1000 and $S_{mn}{\cdot}R_s$=0.01, respectively. For $r = 0.1$, a power penalty of 1 dB is reached with an ICXT level of -23.7 dB and -26.4 dB, for $S_{mn}{\cdot}R_s$=1000 and $S_{mn}{\cdot}R_s$=0.01, respectively. Thus, it can be concluded that, for $r = 0.1$, a lower ICXT level is required to achieve the power penalty of 1 dB. Low $S_{mn}{\cdot}R_s$ requires also a lower ICXT level to achieve this limit than high $S_{mn}{\cdot}R_s$. So, PAM4 systems with high $S_{mn}{\cdot}R_s$ are much more tolerant to ICXT. Furthermore, we have concluded that, compared to OOK systems with direct-detection, the PAM4 systems with direct-detection are much more susceptible to the degradation induced by ICXT.

Finally, the OP of the PAM4 system with direct-detection has been assessed. The OP was estimated considering different parameters scenarios. First, it was shown that the number of MCF realizations required to achieve a sufficiently accurate OP depends mainly on the OP magnitude. The lower the OP, the higher the number of MCF realizations. Then, the OP was studied for λ=1550 nm and one interfering core and, it was concluded that, for the same OP, high $S_{mn}{\cdot}R_s$ tolerates a higher ICXT level than low $S_{mn}{\cdot}R_s$, independently of the extinction ratio. Comparing to OOK optical systems in [38], [43], a much higher ICXT level of about 8.9 dB and 7.6 dB, for high and low $S_{mn}{\cdot}R_s$, respectively, is required to achieve the same OP in the PAM4 system. Again, and as for OOK systems with direct-detection, it has been shown that in PAM4 systems it is essential to

study the OP due to ICXT rather than the power penalty. We have shown that for crosstalk levels that lead to a power penalty of 1 dB, the system is unavailable with a prohibitive probability above 10^{-2}. The dependence of the OP on the chromatic dispersion was also studied for a different fiber transmission window, λ =1310 nm, and D_λ =1 ps/(nm·km) and it was concluded that the system becomes more tolerant to ICXT, because the ICXT levels that lead to the same OP of 10^{-4} are at least 2.5 dB higher than the ones found for λ=1550 nm. This ICXT increased tolerance is attributed to the negligible influence of chromatic dispersion for λ=1310 nm. Then, the dependence of the OP on the number of interfering cores was also assessed, and it has been shown that, by doubling the number of interfering cores, the ICXT level necessary to reach the same OP decreases nearly 3 dB, for a null extinction ratio. For $r = 0.1$, and an OP=10^{-3}, a similar ICXT level degradation of 3 dB is only observed when passing from 2 to 4 interfering cores. Lastly, the dependence of the OP on the time misalignment between signals in the cores was studied and it was concluded that, for high $S_{mn}{\cdot}R_s$, the OP does not depends significantly on the time misalignment. For low $S_{mn}{\cdot}R_s$, a lower OP is reached for a time misalignment between the signals of half the symbol period.

Chapter 5

Conclusions and future work

In this chapter, the dissertation final conclusions and some suggestions for future work are presented.

5.1 Final conclusions

In chapter 2, a literature review of the most important concepts related to this work is presented. In chapter 3, the optical telecommunication equivalent system model of the PAM4 intra-datacenter optical link developed to study the ICXT impairment is presented. This equivalent system model is composed by: the optical transmitter, the dual polarization DCM model that generates the ICXT, considering both signal directions, and the direct-detection optical receiver composed by a PIN photodetector and an electrical filter. The average BER assessment using MC simulation combined with a semi-analytical technique using this equivalent system model is also described. Also, in this chapter, the validation of the BER assessment is performed through the BER estimated analytically and the BER estimated through the Matlab simulation, in a B2B configuration. A very good agreement between BER estimates is found using both methods, which validates our system model and performance assessment in the absence of ICXT.

In chapter 4, the impact of ICXT on the performance of the transmission of PAM4 signals in short direct-detection links, emulating intra-datacenters connections with less than 2 km, is studied and discussed. It has been shown that, about 1000 MCF realizations are necessary to predict the average BER with sufficient accuracy. The eye-patterns have been also analyzed and, it was concluded that, some specific MCF realizations can lead to a severe eye-pattern degradation due to a strong ICXT impact, especially for low $S_{mn}{\cdot}R_s$.

The power penalty due to ICXT is also studied to investigate the degradation caused by the ICXT on the average BER. A threshold power penalty of 1 dB has been defined and it was concluded that, to reach this power penalty, for $r = 0$, a ICXT level of -23 dB and -25.3 dB, is required for $S_{mn}{\cdot}R_s$=1000 and $S_{mn}{\cdot}R_s$=0.01, respectively. For $r = 0.1$, a power penalty of 1 dB is reached with an ICXT level of -23.7 dB and -26.4 dB, for $S_{mn}{\cdot}R_s$=1000 and $S_{mn}{\cdot}R_s$=0.01, respectively. Thus, for $r = 0.1$, a lower ICXT level is required to achieve the power penalty of 1 dB, such as low $S_{mn}{\cdot}R_s$ requires a lower ICXT. It has been also found that PAM4 systems with direct-detection are much more susceptible to the degradation induced by ICXT than OOK systems, by comparison with results presented in other works in the literature.

Finally, the OP of the PAM4 system has been also studied. The results presented shown that the number of MCF realizations required to reach a sufficiently accurate OP solely depends on the OP magnitude. Additionally, the OP for λ=1550 nm and one interfering core has been assessed and it was shown that, for high $S_{mn}{\cdot}R_s$, the system is more tolerant to the ICXT than for low $S_{mn}{\cdot}R_s$ for a reference OP of 10^{-3}. Comparing to OOK optical systems, a much higher ICXT level of about 8.9 dB and 7.6 dB, for high and low $S_{mn}{\cdot}R_s$, respectively, leads to the same OP in PAM4 systems. The dependence of the OP due to ICXT on the chromatic dispersion has been also investigated. The results obtained with λ=1310 nm indicates that the OP is much dependent on the ammount of chromatic dispersion present in the fiber system. For λ=1310 nm, the system tolerates at least 2.5 dB higher ICXT levels than for λ=1550 nm. The dependence of the OP on the number of interfering cores has been also studied, and it has been

shown that by doubling the number of interfering cores, the ICXT level necessary to reach the same OP decreases by about 3 dB, for a null extinction ratio. For $r = 0.1$, the crosstalk level necessary to reach the reference OP decreases approximately 3 dB, when passing from 2 to 4 interfering cores, while when comparing 1 and 2 interfering cores, the OPs estimated are practically the same. Lastly, the study of the dependence of the OP on the time misalignment between signals has been performed. For high $S_{mn} \cdot R_s$, it was concluded that, the OP is practically independent of the time misalignment and, for low $S_{mn} \cdot R_s$, a minimum OP is reached for a time misalignment of half the symbol period.

5.2 Future work

Some future work proposals are presented:

• Study the PAM4 transmission in inter-datacenter connections (with lenght below 100 km) [3] and analyze the impact of ICXT on the performance of that system;

• Improve the performance of the PAM4 system by considering electronic equalization after the optical receiver;

• Proposal and analysis of ICXT mitigation techniques to reduce its impact on the performance of datacenters interconnects;

• Investigation of the transmission of the higher order PAM signals (as PAM8 [49]) to enhance the capacity of datacenter links.

Bibliography

[1] Cisco, "Cisco global cloud index: forecast and methodology, 2016–2021," *White paper*, pp. 1–46, Feb. 1 2018.

[2] X. Zhou, R. Urata, and H. Liu, "Beyond 1 Tb/s datacenter interconnect technology: challenges and solutions," *Optical Fiber Communications Conference and Exhibition (OFC)*, San Diego, CA, USA, Mar. 2019, paper Tu2F.5.

[3] J. Perin, A. Shastri, and J. Kahn, "Data center links beyond 100Gbit/s per wavelength," *Optical Fiber Technology*, vol. 44, pp. 69–85, Aug. 2018.

[4] K. Saitoh and S. Matsuo, "Multicore fiber technology," *Journal of Lightwave Technology*, vol. 34, no. 1, pp. 55–66, Jan. 1 2016.

[5] D. Butler *et al.*, "Space division multiplexing in short reach optical interconnects," *Journal of Lightwave Technology*, vol. 35, no. 4, Feb. 15 2017.

[6] W. Klaus *et al.*, "Advanced space division multiplexing technologies for optical networks," *Journal of Lightwave Technology*, vol. 9, no. 4, pp. 1–11, Apr. 4 2017.

[7] E. Virgillito, "Limitations of PM-QAM based multicore fiber transmission systems due to intercore crosstalk," Master's thesis, Telecommunications engineering, Instituto Superior Técnico, 2016.

[8] T. Alves, J. Rebola, and A. Cartaxo, "Outage probability due to intercore crosstalk in weakly-coupled MCF systems with OOK signaling," *Optical Fiber Communications Conference and Exhibition (OFC)*, San Diego, CA, USA, Mar. 2019, paper M2I.1.

[9] A. Udalcovs *et al.*, "Inter-core crosstalk in multicore fibers: impact on 56-Gbaud/λ/core PAM-4 transmission," *European Conference on Optical Communication (ECOC)*, Rome, Italy, Feb. 2018, paper We2.3.

[10] T. Hayashi, T. Taru, O. Shimakawa, T. Sasaki, and E. Sasaoka, "Design and fabrication of ultra-low crosstalk and low-loss multi-core fiber," *Optics Express*, vol. 19, no. 17, pp. 16576–16592, 2011.

[11] M. Noormohammadpour and C. Raghavendra, "Datacenter traffic control: understanding techniques and trade-offs," *IEEE Communications Surveys & Tutorials*, vol. 20, no. 2, Dec. 14, 2017.

[12] C. Kachris and I. Tomkos, "A survey on optical interconnects for data centers," *IEEE Communications Surveys & Tutorials*, vol. 14, no. 4, pp. 1021–1036, 2012.

[13] S. Beppu *et al.*, "56-Gbaud PAM4 transmission over 2-km 125-μm-cladding 4-core multicore fibre for data centre communications," *European Conference on Optical Communication (ECOC)*, Gothenburg, Sweden, Sep. 2017, paper Th.2.A.2.

[14] L. Zeng, X. Song, J. Man, W. Chen, and W. Zhou, "PAM4 transmission for short reach optical interconnection," *International Conference on Optical Communications and Networks (ICOCN)*, Nanjing, China, Jul. 2015.

[15] B. Teipen, N. Eiselt, A. Dochhan, H. Griesser, M. Eiselt, and J.-P. Elbers, "Investigation of PAM-4 for extending reach in data center interconnect applications," *International Conference on Transparent Optical Networks (ICTON)*, Budapest, Hungary, Jul. 2015, paper Mo.D3.3.

[16] E. El-Fiky, M. Chagnon, M. Sowailem, A. Samani, M. Morsy-Osman, and D. Plant, "168 Gb/s single carrier PAM4 transmission for intra data center optical interconnects," *IEEE Photonics Technology Letters*, vol. 29, no. 3, pp. 314–317, Feb. 1 2017.

[17] J. Perin, *Spectrally and power efficient optical communication systems.* PhD thesis, Electrical Engineering, Stanford University, Jun. 2018.

[18] G. Agrawal, *Fiber-optic communications systems.* John Wiley & Sons, 4^{th} ed., 2010.

[19] Telecommunications Standardization Section of ITU-T, *Optical fibres, cables and system.* Handbooks on Standardization, ITU, Geneva, 2009.

[20] M.-J. Li, "MMF for high data rate and short length applications," *Optical Fiber Communication Conference*, San Francisco, CA, USA, Mar. 2014, paper M3F.1.

[21] T. Hayashi and T. Nakanishi, "Multi-core optical fibers for the next-generation communications," *SEI Technical Review,* no. 86, pp. 23–28, Apr. 2018.

[22] H. Venghaus and N. Grote, *Fibre Optic Communication: Key Devices.* Springer-Verlag, 2^{nd} ed., Berlin, Germany, 2012.

[23] T. Hayashi, T. Nakanishi, O. Shimakawa, F. Sato, T. Taru, and T. Sasaki, "125-Mm-Cladding 8-Core Fiber for Short-Reach Optical Interconnects," *SEI Technical Review,* no. 83, pp. 21–25, Oct. 2016.

[24] K. Takenaga, S. Tanigawa, N. Guan, S. Matsuo, S. K, and K. M, "Reduction of crosstalk by quasi-homogeneous solid multi-core fiber," *Optical Fiber Communication*, San Diego, CA, USA, Mar. 2010, paper OWK7.

[25] T. Alves and A. Cartaxo, "Intercore crosstalk in homogeneous multicore fibers: theoretical characterization of stochastic time evolution," *Journal of Lightwave Technology*, vol. 35, no. 21, p. 4613–4623, Nov. 1 2017.

[26] G. Rademacher, R. Luís, B. Puttnam, Y. Awaji, and N. Wada, "Crosstalk dynamics in multi-core fibers," *Optics Express*, vol. 25, no. 10, May. 15 2017.

[27] N. Eiselt *et al.*, "Experimental demonstration of 56 Gbit/s PAM-4 over 15 km and 84 Gbit/s PAM-4 over 1 km SSMF at 1525 nm using a 25G VCSEL," *European Conference on Optical Communication (ECOC)*, Dusseldorf, Germany, Sep. 2016.

[28] Y. Shen *et al.*, "Generation of PAM4 signal over 10-km multi core fiber using DMLs and photodiode," *International Conference on Advanced Infocomm Technology (ICAIT)*, Chengdu, China, Nov. 2017.

[29] O. Ozolins *et al.*, "7×149 Gbit/s PAM4 transmission over 1 km multicore fiber for short-reach optical interconnects," *Conference on Lasers and Electro-Optics (CLEO)*, San Jose, CA, USA, May. 2018, paper SM4C.4.

[30] W. Lv, J. Li, and K. Xu, "Direct detection of PAM4 signals with receiver side digital signal processing for bandwidth-efficient short-reach optical transmissions," *IEEE Optoelectronics Global Conference (OGC)*, pp. 4–6, Shenzhen, China, Sep. 2016.

[31] J. Rebola, C. Lourenço, and J. Oliveira, "Projecto e simulação de um sistema de comunicação óptica de muita alta velocidade," Final year project of degree in Electrical Engineering and Computers, Instituto Superior Técnico, Set. 1999.

[32] J. Rebola, "Optimização de um sistema de comunicação óptica quaternário com níveis não equidistantes," Research project report, Instituto Superior Técnico, Dec. 1999.

[33] R. O. J. Soeiro, T. M. F. Alves, and A. V. T. Cartaxo, "Dual polarization discrete changes model of inter-core crosstalk in multi-core fibers," *IEEE Photonics Technology Letters*, vol. 29, no. 16, pp. 1395–1398, Aug. 15, 2017.

[34] A. V. T. Cartaxo, R. S. Luís, B. J. Puttnam, T. Hayashi, Y. Awaji, and N. Wada, "Dispersion impact on the crosstalk amplitude response of homogeneous multi-core fibers," *IEEE Photonics Technology Letters*, vol. 28, no. 17, pp. 1858–1861, Sep. 17 2016.

[35] H. Baher, *Analog & digital signal processing.* John Wiley & Sons, 1^{st} ed., England, 1990.

[36] A. Carlson and P. Crilly, *Communication Systems - An introduction to signals and noise in electrical communication.* McGraw-Hill International Editions, 5^{th} ed., New York, USA, 2010.

[37] R. Srivastava and N. Dixit, "Numerical accuracy of bisection method ," *International Multidisciplinary Research Journal*, vol. 2, no. 1, 2012.

[38] J. Rebola, A. Cartaxo, and A. Marques, "10 Gbps CPRI signals transmission impaired by intercore crosstalk in 5G network fronthauls with multicore fibers," *Photonic Network Communications*, vol. 37, no. 3, pp. 409–420, Jun. 2019.

[39] N. Eiselt *et al.*, "Experimental demonstration of 84 Gb/s PAM-4 over up to 1.6 km SSMF using a 20-GHz VCSEL at 1525 nm," *Journal of Lightwave Technology*, vol. 35, no. 8, pp. 1342–1349, Apr. 15 2017.

[40] T. Alves and A. Cartaxo, "Decorrelation bandwidth of intercore crosstalk in weakly coupled multicore fibers with multiple interfering cores," *Journal of Lightwave Technology*, vol. 37, no. 3, pp. 744–754, Feb. 1 2019.

[41] J. Rebola, T. Alves, and A. Cartaxo, "Assessment of the combined effect of laser phase noise and intercore crosstalk on the outage probability of DD OOK systems," *International Conference on Transparent Optical Networks (ICTON)*, Angers, France, Jul. 2019, papper We.D1.4.

[42] M. Chagnon, S. Lessard, and D. Plant, "336 Gb/s in direct detection below KP4 FEC threshold for intra data center applications," *IEEE Photonics Technology Letters*, vol. 28, no. 20, pp. 2233–2236, Oct. 15 2016.

[43] A. Marques, "Transmission of 5G signals in multicore fibers impaired by intercore crosstalk," Master's thesis, ISCTE - Instituto Universitário de Lisboa, Oct. 2018.

[44] A. Souza, R. Figueiredo, J. Hélio, S. Rossi, and A. Chiuchiarelli, "Extended-reach transmission of single-wavelength 112-Gbps PAM4 channel enabled by

MLSE for intra data center applications," *International Microwave and Optoelectronics Conference (IMOC)*, Aguas de Lindoia, Brazil 2017.

[45] J. Rebola, A. Cartaxo, T. Alves, and A. Marques, "Outage probability due to intercore crosstalk in dual-core fiber links with direct-detection," *IEEE Photonics Technology Letters*, vol. 31, no. 14, pp. 1195–1198, Jul. 15 2019.

[46] P. Winzer and G. Foschini, "MIMO capacities and outage probabilities in spatially multiplexed optical transport systems," *Optics Express*, vol. 19, no. 17, pp. 16680–16696, Aug. 15 2011.

[47] N. Cvijetic, S. Wilson, and D. Qian, "System outage probability due to PMD in high-speed optical OFDM transmission," *Journal of Lightwave Technology*, vol. 26, no. 14, pp. 2118–2127, Jul. 15 2008.

[48] R. Luís *et al.*, "On the spectral efficiency limits of crosstalk-limited homogeneous single-mode multi-core fiber systems," *Proceedings Advanced Photonics*, New Orleans, Louisiana, USA, Jul. 2017, paper NeTu2B.2.

[49] S. Gaiarin *et al.*, "High speed PAM-8 optical interconnects with digital equalization based on neural network," *Asia Communications and Photonics Conference (ACP)*, Nov. 2016, paper AS1C.1.